Electrochimica Acta 354 (2020) 136663

Contents lists available at ScienceDirect

Electrochimica Acta

journal homepage: www.elsevier.com/locate/electacta

Electrochemical performance of Silsesquioxane-GO loaded with alkoxy substituted ammonium-based ionic liquid and POAP for supercapacitor

Farshad Boorboor Ajdari [a], Elaheh Kowsari [b, *], Hamid Reza Nadri [c], Mahdie Maghsoodi [b], Ali Ehsani [d], Hamid Mahmoudi [e], Saeideh Kholghi Eshkalak [f], Amutha Chinnappan [g], W.A.D.M. Jayathilak [g], Seeram Ramakrishna [g]

[a] Department of Applied Chemistry, Faculty of Chemistry, University of Kashan, Kashan, Iran
[b] Department of Chemistry, Amirkabir University of Technology (AUT), Tehran, Iran
[c] Novin Ebtekar Company, Exclusive Agent of Metrohm-Autolab and Dropsens Companies, East Hagh Talab St., South Allame St.9 Saadat abad Ave., Tehran, 1997834991, Iran
[d] Department of Chemistry, Faculty of Science, University of Qom, Qom, Iran
[e] Department of Chemistry, Faculty of Science, University of Kurdistan, Zip Code, 66177-15175, Sanandaj, Iran
[f] Department of Polymer Engineering and Color Technology, Amirkabir University of Technology, Tehran, Iran
[g] Department of Mechanical Engineering, Center for Nanofibers and Nanotechnology, National University of Singapore, 119260, Singapore

ARTICLE INFO

Article history:
Received 15 March 2020
Received in revised form
18 June 2020
Accepted 21 June 2020
Available online 12 July 2020

Keywords:
Alkoxy substituted ammonium-based ionic liquid
Poly ortho amino phenol
Supercapacitors

ABSTRACT

Recently, the electrochemical efficiency of supercapacitors has experienced a dramatic rise, followed by a rapid developing rate on introducing promising electrode material, led to manufacture highly performance supercapacitors. In this work we synthesized Silsesquioxane -containing graphene oxide (SSQ-GO) and alkoxy substituted ammonium-based ionic liquid, (Tris[2-(2-methoxy ethoxy) ethyl]methyl ammonium Iodide (TMEMAI)) blended with conductive polymer, Poly ortho amino phenol (SSQ-GO-TMEMAI-POAP) used as an electrode in both three and two-electrode systems. The prepared material characterized by XPS, XRD, TEM, SEM, EDX, techniques and the attributed electrochemical tests carried out by cyclic voltammetry, chronopotentiometry techniques. The incorporating of TMEMAI into GO surface with porous structure in the presence of conductive polymer exhibited high conductivity and decreased resistance through the efficient electron channels based on electrochemical impedance spectroscopy test. The specific capacitance and energy density of SSQ-GO-TMEMAI-POAP were significantly improved, while retention capacity obtained ~96% within 3000 charge-discharge cycles, with high durability. Concerning the two-electrode design, the specific capacitance calculated as 450 F g^{-1} at 0.5 A g^{-1}, where the energy density at power density achieved of 22.5 W h kg^{-1}, 300 W kg^{-1}, respectively. The incorporation of ionic liquid and conductive polymer within SSQ-GO-TMEMAI-POAP nanocomposite indicated high electrochemical potential where used in energy storage devices.

1. Introduction

With the increasing demands for global clean energy, portable and affordable devices, ease accessible and friendly environmental energy storage systems, a substantial expansion of research has been sacrificed to develop electrochemical super(ultra)capacitors towards introducing high reliable supercapacitors (SCs) with perfect efficiency in the field of electrochemical storage [1–5]. In our world, batteries have been widely used in various applications and they have become more popular with the beneficial of high energy density, cost effectiveness and good lifespan [6–8]. In contrast to batteries, supercapacitors enjoy from significant power density, considerable lifetime, striking fast charge-discharge period with high cyclability but low energy density which limited their wide commercial applications in different industries. While it suggests a high research potential to expand effective strategies to overcome inherent drawbacks and improve the amount of energy

* Corresponding author.
E-mail address: Kowsarie@aut.ac.ir (E. Kowsari).

https://doi.org/10.1016/j.electacta.2020.136663
0013-4686/

stored per unit volume. Regarding to the main energy storing mechanisms of SCs including EDLC and pseudocapacitance, a large number of researchers developed high performance SC devices [9–13]. Basically, the separation of ionic and electronic charges in the electrolyte and electrode interface describes an EDLC, founded in carbon-based materials such as activated carbon, graphene, carbon aerogel, CNT [14–17]. When the charges store through arising within the active material of the electrodes (Faradaic reactions), it defines pseudocapacitor system contributed to conductive polymers and metal oxides [5,18–21]. To improve the electrochemical features in the lights of specific capacitance, power density, and energy density, the designing and preparing promising electrode materials using concurrent EDLC and pseudocapacitance (hybrid mechanism) are desirable manner. To conduct the high capacity, graphene oxide (GO) and graphene as an allotrope of carbon with different functional groups or their derivatives, and fabricating nanocomposite ternary provide high electrochemical efficiency in case of ultracapacitors due to presenting wide potential window, outstanding electrical conductivity in plane, and large surface area [22–29]. For instance, the reduced graphene oxide (rGO) was used as an electrode in organic and aqueous KOH environment in SC with respect specific capacitance of 100 and 130 F g^{-1} [30]. Hybrid designed of graphene-polyaniline electrode containing sulfonated (SG) and aminated graphene mixed by polyaniline (PANI) with different morphologies and structures and conducive to the vertical and neat growth of PANI nanorods were evaluated electrochemically in which high ion/electron transporting pathways with a major ion-accessible surface area in the presence of $-SO_3$ groups that accelerated the redox reaction through (de)doping of the PANI. Thus, the specific capacitance reached to 863.2 F g^{-1} (@ 0.2 A g^{-1}) [24]. Electrodes of MnO_x-rGO nanocomposites in asymmetric supercapacitor showed a specific capacitance of 183 F g^{-1} during a scan rate of 5 mV s^{-1}, with 98% capacity retention within 10^4 charge/discharge cycles (@ 2 A g^{-1}) with energy and power density of 16.6 Wh kg^{-1} and 1.052 kW kg^{-1} (@ 1 A g^{-1}) based on hybrid mechanism [31]. Besides, $NiCoO_2$@rGO/NF nanocomposite exhibited an outstanding capacitance (1970 F g^{-1}) with excellent retention (102%, @ 2500 cycles) in which employed in asymmetric supercapacitor (ASC) and the energy and power density achieved as 42.3 Wh kg−1 and 0.4 kW kg^{-1}, respectively [32]. Furthermore, to improve the conducting and facilitating the electron passing through the channels, ionic liquids (ILs) as organic salts in ionic state with melting point around ambient temperature showing high potential to enhance the electrochemical terms. Hence, ionic liquids with organic cations and various anions provide negligible vapor pressure, wide electrochemical widow, high electrochemical and thermal stability, highly tunable, safe, and non-flammable features [33–37]. Among different types of ILs, Imidazolium-based are quite trendy for energy storage image and a bit more obsessed where used in electrolyte due to high electron conductivity. When it comes to electrode materials, ionic liquids with purpose-built porous carbon structures, dramatically award improved electrochemical efficiency [38–41]. For instance, an electrode film of freestanding cellulose nanofibril-rGO-molybdenum oxynitride aerogel was developed to employ in all-solid-state SC with specific capacitance and energy density of 518 F g^{-1} and 114 Wh kg^{-1}, respectively [42]. In our previous works we developed functional graphene oxide with synthesized IL-235 and IL-178 ionic liquids, melamine (N enrichment), and $-SO_3$ molecules and then conjugated with poly ortho amino phenol (PAOP) as a promising conductive polymer to employ in three electrode ultracapacitor. Based on the results and reported papers, the functionalized GO with metal fabricating and conductive polymers due to presenting a synergistic electrochemical effect can be used as an eminent electrode material in SCs [43–46].

Here in, we synthesized an ionic liquid of Tris[2-(2-methoxy ethoxy) ethyl]methyl ammonium chloride (TMEMAI) to composite with graphene oxide and further electrochemical investigating carried out by compositing ionic liquid and functional graphene oxide. Hence, SSQ-[3-(2-Aminoethyl) amino] propyl-Heptaisobutyl substituted (SSQ) molecule grafted on carbon-based graphene oxide structure while enriched by O—Si—*O*- bonds with chemical reactions and then well considered the influence of silicon containing GO surface on supercapacitor performance in a three-electrode setting. By characterization and confirming the prepared ionic liquid TMEMAI, SSQ-GO structure by NMR, XPS, XRD and Rietveld analysis. The SSQ-GO and TMEMAI composite then interwoven by conductive POAP to make SSQ-GO-TMEMAI-POAP electrode film and determined to enhance the electrochemical features through presenting hybrid EDLC/pseudocapacitance mechanism with accelerating electron transport through the pathways. The electrochemical tests were carried out based on the two/and three-electrode systems to consider the cyclic voltammetry (CV), galvanostatic charge-discharge (GCD) and electrochemical impedance spectroscopy (EIS) properties. The as-prepared nanocomposite improved the specific capacitance and energy density based on the charge-discharge (C-D), galvanostatic analysis and EIS tests.

2. Operating process, synthesis and preparation method

2.1. Materials

All materials used in this investigation including Graphite powder (powder, ≥99.99%, <45 μm, Sigma-Aldrich), SSQ-[3-(2-Aminoethyl)amino]propyl-Heptaisobutyl substituted, Methyl Iodide, Tris[2-(2-methoxy ethoxy) ethyl]methyl amine, THF, $NaNO_3$ (≥99.0%, 84.99 g mol^{-1}), H_2SO_4 (95%, pure), $KMnO_4$ (158.03 g mol^{-1}, pure), H_2O_2, HCl, $SOCl_2$, and SSQ was purchased from Sigma Aldrich company with three times distilled water.

2.2. Ionic liquid synthesis

To prepare the ionic liquid, firstly, Methyl Iodide (MeI; 5 ml) was added to a three-necked flask equipped with a pipe dryer and funnel located in an ice bath. Then Tris[2-(2-methoxy ethoxy) ethyl]methyl amine (10 ml) was gradually added into the flask with constant stirring. The reaction of was continued until the ice bath reached the room temperature. The exceeded MeI was evaporated and a viscose brown liquid was obtained as Tris[2-(2-methoxy ethoxy) ethyl]methyl ammonium Iodide ionic liquid (TMEMAI) and washed with Diethyl ether and dried under vacuum with the yield of 55% Fig. 1 shows the schematic structure of synthesized ionic liquid TMEMAI. Moreover, the structure of TMEMAI was characterized by FT-IR, ^{1}H NMR and ^{13}C NMR techniques as following:

FT-IR: (NaCl plate, cm^{-1}), (C—O: 1111 cm^{-1}), (C—C: 1458 cm^{-1}),

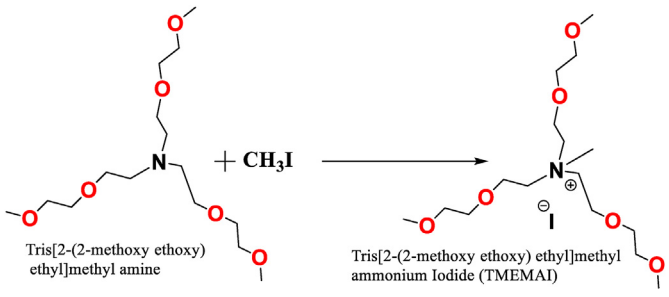

Fig. 1. Schematic structure and synthesis of synthesized ionic liquid TMEMAI.

(C—H: 2885 cm^{-1}). **^{1}H NMR:** (acetone-d6, δ) 3.30 (s, 9H, OCH_3), 3.42 (s, 3H, NCH_3), 3.57 (m, 6H, $N(CH_2CH_2OCH_2CH_2OCH_3)_3$), 3.70 (m, 6H) $N(CH_2CH_2OCH_2CH_2OCH_3)_3$), 4.00 (m, 12H) $N(CH_2CH_2OCH_2$-$CH_2OCH_3)_3$). **^{13}C NMR:** (300 MHz, acetone-d6, ppm) 51.12, 58.80, 63.90, 65.50, 70.83, 72.35. Anal. Calcd. For $C_{16}H_{36}INO_6$: C, 41.29%; H, 7.80%; N, 3.01%. Found: C, 41.05%; H, 7.63%; N, 2.90%

2.3. Preparation of graphene oxide and SSQ-GO

In this study, graphene oxide was prepared based on the modified Hummer's procedure described in Ref. [47–49]. Typically, both $NaNO_3$ (1.25 g) and graphite powder (2.5 g) were added to an acidic solution of H_2SO_4 (60 ml) in which a round-bottom flask was used in an ice bath for half an hour. Then, $KMnO_4$ (7 g) as a strong oxidizing agent was included in solution with slow Shuffling (12 h) and this stirring followed by adding distilled water (150 ml) where the temperature reached at 96 °C. Furthermore, the stirring was continued for another 24 h and then H_2O_2 (30%, 50 ml) was added slowly with 300 rpm stirring rate. The obtained light black powder was washed repeatedly with H_2O and HCl and dried in vacuum oven (100 °C). To fabricate functions on graphene oxide surface, the prepared GO (2 g) was refluxed in thionyl chloride ($SOCl_2$) during 4 h and then the excess $SOCl_2$ was removed and then the acylated graphene oxide (AcGO) was filtrated and washed regularly with dichloromethane solution (CH_2Cl_2, 40 ml). Thereafter, AcGO (2 g) was dispersed in Tetrahydrofuran (THF, 50 ml) and followed by refluxing (2 h) and then, SSQ powder was added to the mixture and refluxed for 24 h at 65 °C to produce SSQ-GO. in the next step by filtration, the obtained black powder was washed frequently by CH_2Cl_2 (40 ml) and then freeze dried. the obtained product was dried again in room temperature and sealed in a bottle. Fig. 2 represents the schematic framework and preparing process of SSQ-GO composite.

3. Operating electrochemical test

To evaluate the attribute electrochemical nature of prepared materials as electrode, we used Autolab potentiostat (PGSTAT 302 N).

Preparation of Working Electrodes in Supercapacitor. To adjust the working electrodes, the SSQ-POAP, SSQ-GO-POAP, and SSQ-GO-TMEMAI-POAP were separately mixed with graphite, carbon black, and PTFE as a ratio of 70:10:15:5, respectively. Then, to obtain a homogeneous muddle, a little of ethanol was added to the mixture. Thereafter, the mixture under a pressure of 10 M Pa, was pressed on a piece of a stainless-steel current collector (1 cm × 1 cm). The loading mass of all the electrodes was maintained at the same level to minimize the test deviation with about 5 mg deposited into the current collector. Concerning the symmetric supercapacitor (SSC) evaluations, SSQ-GO-TMEMAI-POAP was fabricated as both cathode and anode electrodes thanks to stainless steel cell, where electrodes were separated through a polypropylene sheet in 3 M KOH electrolyte.

Electrochemical Measurement. The electrochemical measurements of the three-electrode system were accurately analyzed, in which a Pt and Ag/AgCl were used as a counter and reference electrodes, respectively. Dealing with the three-electrode system, CV, GCD, and EIS were included. For symmetric electrochemical investigations of electrode manufactured by SSQ-GO-TMEMAI-POAP in the supercapacitor, CV, and GCD measurements were done using an Autolab potentiostat (PGSTAT 302 N), at 25 °C in 3 M KOH electrolyte.

4. Characterization

4.1. EDX, FE-SEM, and TEM

To understanding the presenting atoms, morphology and the atomic structure of the as-synthesized SSQ-GO composite, energy-dispersive X-ray (EDX: 15 Kv, 2.562 nA, JEOL JSM-6701 F), field emission scanning electron microscopy (SEM: (Hitachi S4160, Cold Field Emission; 30 kV)) and transmission electron microscopy (TEM: JEM21-00 F)) techniques were employed. As demonstrated in Fig. 3 the percentage of existed atoms and their distribution in the functioned material has changed rather than pure graphene oxide (C, O) concerned of added Si and O atoms, as well as new created links which affected the engaged {hkl} planes. The functioning of SSQ had a striking effect on the morphology and structure of GO sheets with less accumulation and preventing graphene oxide layers restacking as it seen in TEM and FE-SEM (at 5 kV) results (Fig. 4).

4.2. X-ray diffraction patterns and rietveld analysis

To evaluate the structure of as-prepared SSQ-containing composite, the X-ray diffraction (XRD) technique was used (Fig. 5A) and the interpretation of results was supported by further Rietveld refinement analyses through Jacobian matrix which fully ascribed in supplementary information section (word file SI). In this work the XRD characterization carried out by (INEL; (hυ: 1.541874 A), Equinox 3000, Cu- K_α radiation, I: 30 mA, 40 kV). Based on the Rietveld refined data, a significant goodness of fit was obtained for the XRD pattern (Fig. 5B). Additionally, in comparison to the experimental template, the fitting profile (Fig. 5C) represents an extremely low difference (great matching) based on the criterion of crystallographic matching and experimental data in terms of Datafile 1.xy: R_{wp}: 0.039, R_p: 0.031, R_{wpb}: 0.038, R_{pb}: 0.029, while the residual profile (Fig. 5D) describing the available data in the experimental profile, which is not in the fitting pattern demonstrated that Rietveld refinement has been able to provide a specifically good estimate for XRD data fitting [50–55]. Through further crystallography data exploration of reflection pattern, the other useful parameters in the lights of {h k l}, multiplicity of plates, the average FWHM (meanFhkl), crystallite size and micro-strain were extracted contributed to -*O*-Si-*O*- and GO frameworks listed in Table SE1 and SE2. In the crystal structure simulation, the different peaks position with d-spacing were obtained representing the location of lattice sheets in which each peak has a d-spacing indicating a class of lattice planes. Also, peaks possess a defined intensity that represents the relative diffraction strength varying from other peaks. Conventionally, in the pattern of diffractions the strongest peak assigned as main intensity criteria (100%) to relative scale the intensity of other caps. Nevertheless, calculating the region under the peaks (minus background) gives more accurate intensities in which the different estimated intensities can be critically described by scattering intensity variations and their arrangement in crystal structure. Besides, the interference between appeared diffractions contributed to some significant variations with representing chiefly reduced intensities or systematic extinctions in lattice planes. Basically, by increasing the amount of micro-strain due to packing factor rising, the plate (h k l) with the highest strain has more interfacial reaction with the guest molecules or sometimes but not always, pages possessing much similar hkl are more likely to come closer or react more responsibly on those pages. It's like closing up the two ends of the plastic that when the two sides are approaching and a more strain occurs in that area and therefore, the co-deposition of Si—O system can affect the morphology and crystal orientation of the matrix surface.

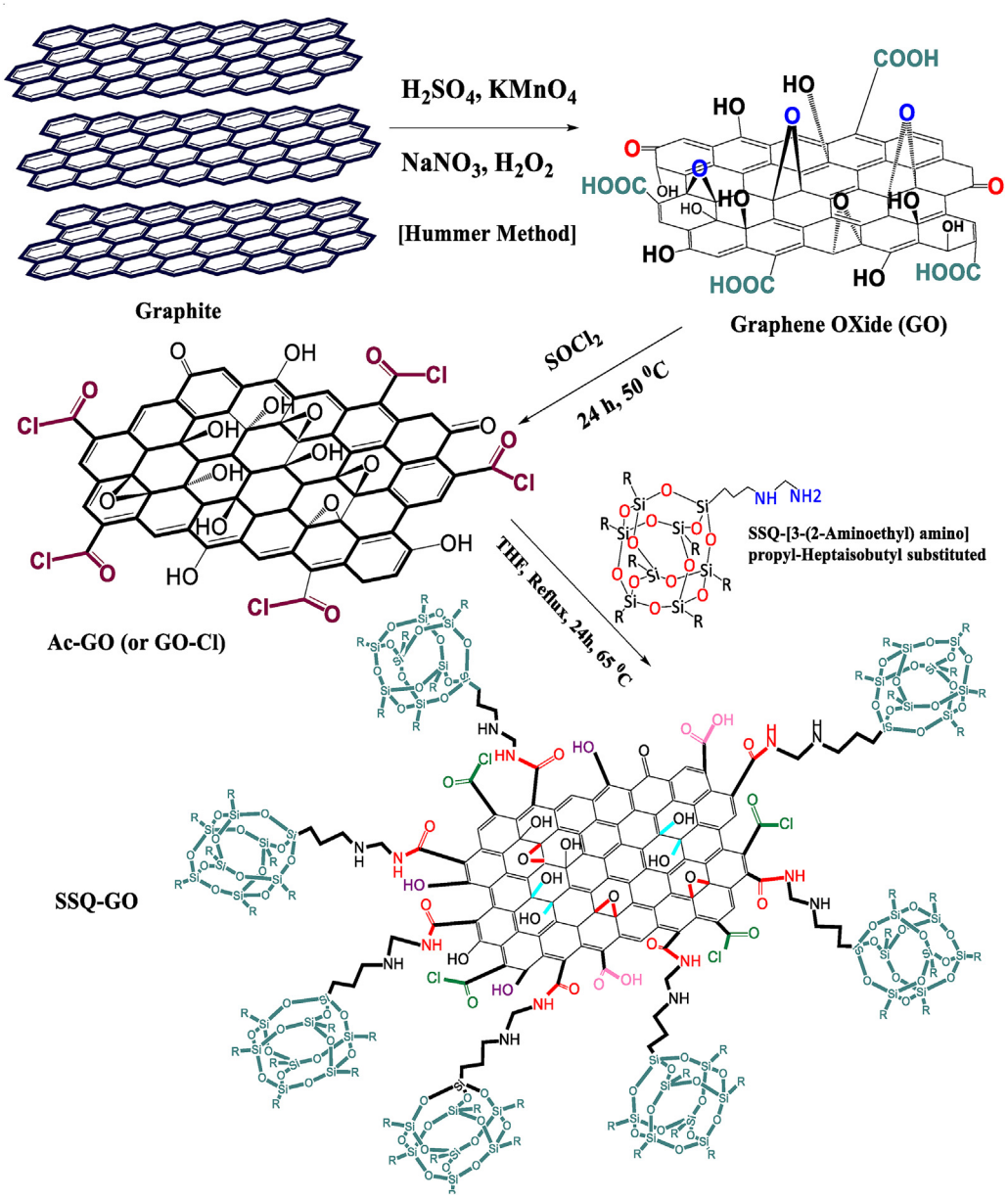

Fig. 2. Schematic structure and preparation method of functional reduced graphene oxide (SSQ-GO).

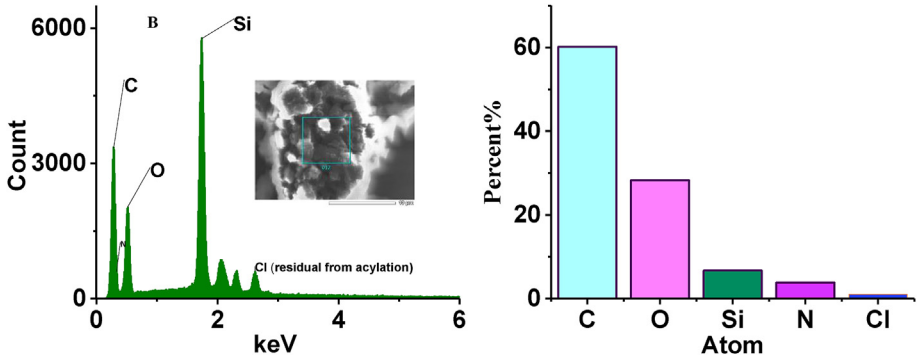

Fig. 3. EDX spectra and the percentage of presented atoms in functional SSQ-GO.

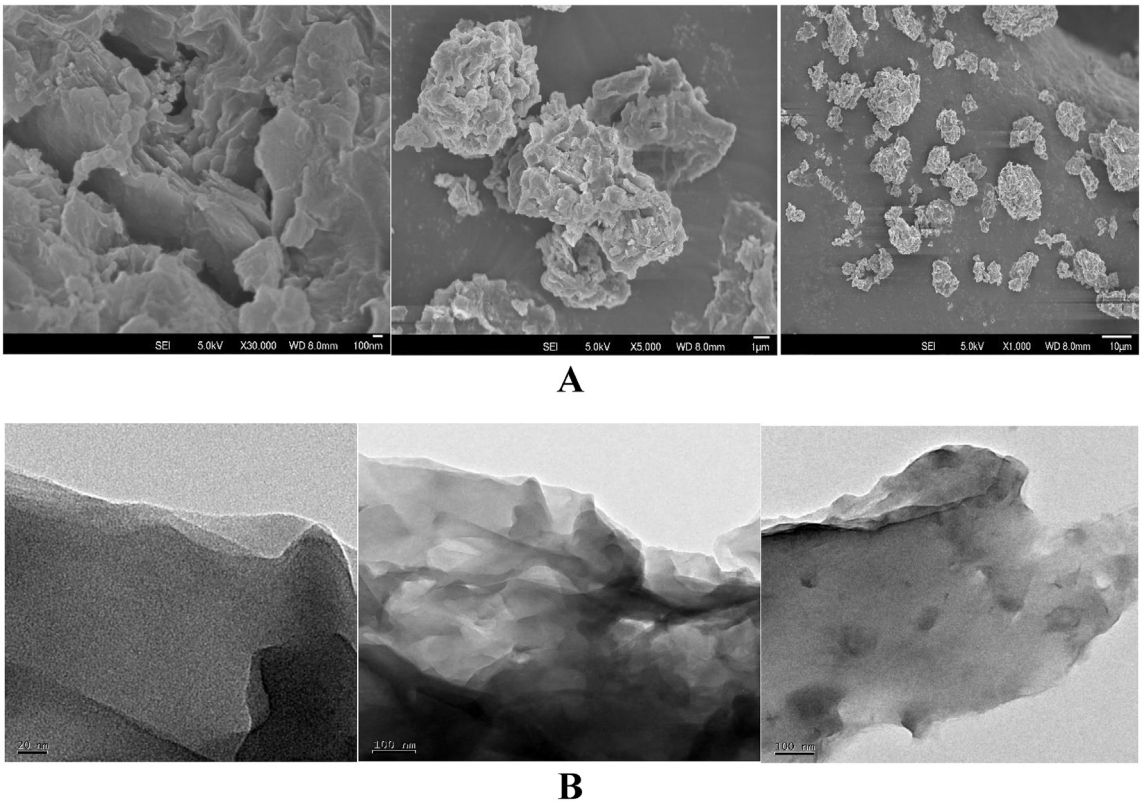

Fig. 4. A) FE-SEM images for morphology of SSQ-containg graphene oxide at 100 nm, 1 μm, and 10 μm, and B) TEM images of SSQ-graphene oxide surfce at 20 nm and 100 nm.

Further useful data reported in this Rietveld analysis is microstrain parameter. The strain in synthesized sample contributed basically to two type of strain including macrostrain and microstrain. The uniform strain (either compressive and tensile) defined as macrostrain with producing larger/smaller cell distances leading to diffraction shifting and changing lattice parameters causing a peak shift. While, micro-strain attributed to distribution of compressive and tensile forces representing a broad diffraction peak with this fact that the micro-strain can produce some peak symmetry. Moreover, the vacancies, dislocations, shear planes, etc., in crystal structure may attributed to micro-stress resulting in appearing of peaks over the unstressed peak location and form a crude broadening peak pattern. Furthermore, the plane multiplicity factor provides useful information concerning the number of identically spaced planes cutting a unit cell attributing particularly to a single hkl group as it be always be low dealing with low symmetry systems. While, a single group of planes in a high symmetry system, can be duplicated by symmetry operations repeatedly so that each "duplicate" contributed to enhancing the diffraction intensity. Among different estimated reflection sheets of Si–O structure [51,56–59], the reflection of {302}, {202}, {201}, and {101} are more under micro-strain and peaks at {220}, {102} and {111} claiming that the crystal structure of silicon experienced less transformation during the synthesis process [60]. And when it comes to GO template, the sheets of {100}, {110}, {200}, and {021} affected by greater pressure. Moreover, based on the Rietveld refinement calculations the density and weigh% of silicon oxide texture and GO structure were computed as 3.87, 61.184 and 1.75, 38.815 respectively, in which by dividing the obtained wt% over the density, the volume% of each proposed structure will be obtained (Table SE3). As it expected the silicon oxide experienced higher wt% but low volume compared to carbon-based framework [61–64].

4.3. X-ray photoelectron spectroscopy (XPS)

The structure and elemental composition with existing bonds of graphene oxide and SSQ-GO were evaluated by X-ray photoelectron spectroscopy (XPS) technique. Based on the deconvolution of measured XPS data (Al-K_α radiation (hυ:1486.6 eV), 107 Pa), the observed bonds confirmed the successful functioning of graphene oxide through making –C═N- links. Therefore, the presented binding energy of graphene oxide indicated in Fig. 6A in which shows 284.7, 286.1, 286.8, 287.6 and 288.4ev contributed to C–C/C═C, C–OH, C–*O*–C, C═O and O═C–O bonds in graphene oxide respectively. When it comes to synthesized silicon containing materials, the binding energy appeared at 284.3 (C–O), 283.7 (C–Si), 285 (C–Si–O), 285.8 (C–N), 286.4 (C–*O*–C), 286.9 (C═O), and 287.5ev (O–C═O) dealing with created bonds in functional template (Fig. 6B). Based on the XPS results, it turns out that existence of N atoms which is desirable for charge transfer at the interface as well as improving conductivity involved in the framework of SSQ-GO. Moreover, SSQ molecules that covalently grafted on carbon template with additional Si–*O*–C and Si–C formed in the sp^2 hybrid and low energy tail of Si–O spectra can affect the electrochemical properties of electrode materials compared to pure GO [31,65–67].

5. Electrochemical measurements

CV measurements: To understand the potential application of the as-synthesized samples in a supercapacitor, the SSQ-POAP, SSQ-GO-POAP, and SSQ-GO-TMEMAI-POAP were orderly employed as a working electrode to record CVs at 50 mV s^{-1}, shown in Fig. 7.a. The working electrodes presented an appropriate potential window between −0.6 and +0.6 V. As can be seen, the ionic liquid-

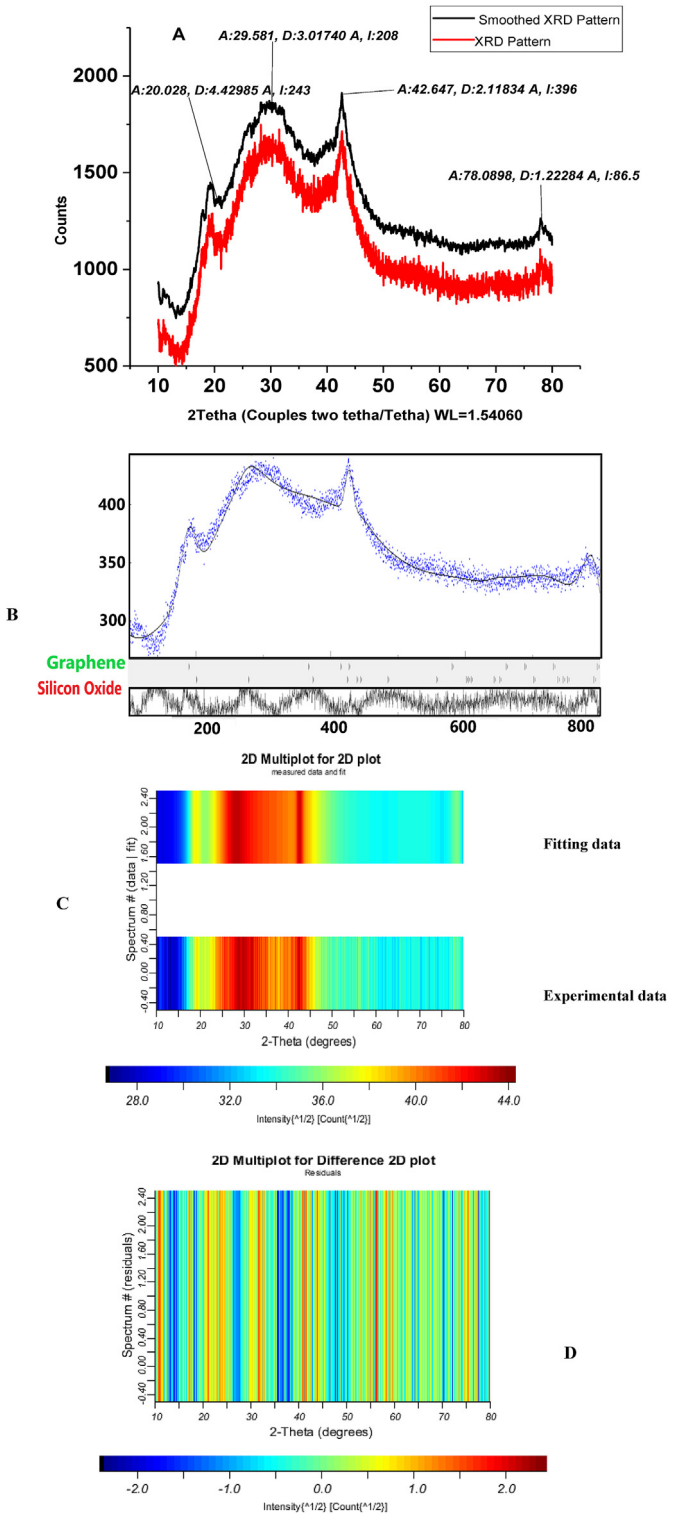

Fig. 5. A) XRD and smoothed XRD pattern, B) Fitting data analysis on XRD pattern, C) Comparison data for fitting and experimental data, and D) Residual data.

containing sample (SSQ-GO-TMEMAI-POAP) distinctly presented wider current density which is describing a significant contribution to electrochemical capacitance, when it compared with two other counterparts. The peaks around 0.2 V are related to quasi-reversible process, indicating a reduction/oxidation of POAP which are then disappeared in SSQ-GO-TMEMAI-POAP due to the highly extended current density span. During the reverse scan process, through an anodic process without attributed cathodic functions, hydroxyl groups of OAP oxidized and by a continuous current raising with further amine group oxidation, the OAP polymerized. Within the first cycle, by origination of cyclic dimer of OAP and 3APZ (3-aminophenoxazone) which followed by a consecutive potential scanning, the current response of this pair of redox peaks progressively arose and a new pair of cathodic redox peaks appeared due to the POAP redox (oxidation/reduction), confirming the formation of polymeric species [68]. Finally, the ortho amino phenol (OAP) was irreversibly oxidized (@600 mV) so that the peak current of SSQ-GO-POAP film showed higher area rather than pure POAP. Originally, protons (H^+) were produced through OAP units coupling with originating cations and radicals, describing desirable EC process for basic polymerization solutions [69].

The CV was regularly performed at different sweep rates ranged from 5 to 75 mV s^{-1} for SSQ-POAP, SSQ-GO-POAP, and SSQ-GO-TMEMAI-POAP samples illustrated in Fig. 7b-d. Interestingly, the CV outlines remain quasi-rectangular shape, when the sweep rate goes orderly up from 5 to 75 mV s^{-1}, describing a desirable capacitive behavior and rate capabilities. Concerning the CV diagrams, appearing a rectangular shape is a sign of ideal electrochemical behavior. An increase in electron transfer and a decrease in charge transfer resistance lead to improved ion diffusion phenomenon. Thus, among three different employed working electrodes, the SSQ-GO-TMEMAI-POAP showed more ideal rectangular shape, pretending more ideal capacitive performance due to high impact of ionic liquids in facilitating electron movements and may contributed to the interconnected 3D pore network created in the KOH activation process. As can be observed in Fig. 7.e, by increasing the sweep rate from 0 to 200 mV s^{-1}, the attributed specific capacitance of each sample was decreased. According to the results, the specific capacitance of SSQ-POAP, SSQ-GO-POAP, and SSQ-GO-TMEMAI-POAP electrodes was decreased from 443, 560, and 722 F g^{-1} to 246, 347, and 478 F g^{-1} at the scan rate of 200 mV s^{-1}, respectively. Dealing with the highest efficiency of SSQ-GO-TMEMAI-POAP electrode, the specific capacitance experienced 33.7% capacitance loss. The improved efficiency of SSQ-GO-TMEMAI-POAP can be attributed to the improved surface area because of the different types of treatments, an increase in redox reaction in outer surface of the SSQ-GO-TMEMAI-POAP electrode. Also, the adequate pathway and enough time for moving electrolyte ions into the available porous structures, which may originate from enhanced electrochemical conductivity as well as treatment procedures [70,71].

By enhancing the range of applied potential in CV test a broad screen was observed that may attributed to improved conductivity with good mass transport and lower equivalent series resistance. Also, the fractal concept is a parameter to study the morphology of synthesized composites through equation (1). Ideally, by plotting the logarithm measures of current-potential (I–V) the slope of the drawn line represents the fractal parameter ($\propto$) and then by substituting in Equation (1), the fractal dimension (D_f) was obtained as 3.6 and 3.2 for SSQ-GO-POAP and SSQ-GO-TMEMAI-POAP, describing a porous structure in morphological framework with improving the electrode features [43,46,72,73].

$$\propto = \left(D_f - 1\right) / 2 \tag{1}$$

5.1. GCD measurement

The further electrochemical analysis was performed by the GCD method as a trustworthy technique under authored conditions to

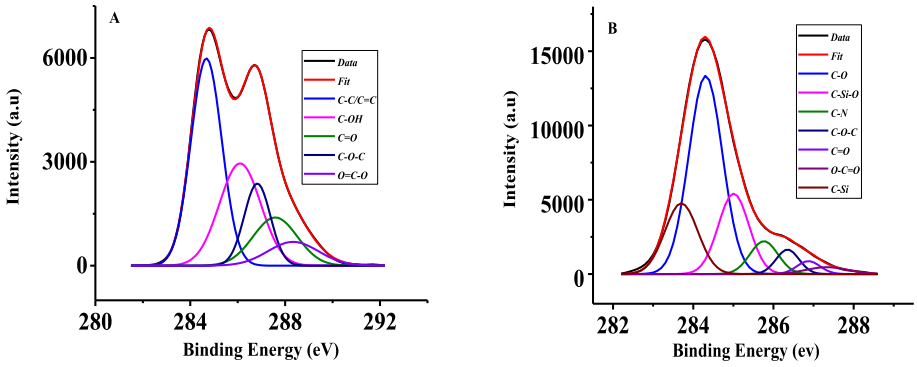

Fig. 6. The XPS spectra and deconvolution data of C1s with their involving bonds of A) graphene oxide and B) functionalized SSQ-GO.

understand the electrochemical features. Fig. 8.a exhibits the GCD diagrams for all three prepared samples at a current density of 2.0 A g^{-1}, which are symmetric, triangular-shaped, linear, and moderately sharp. This comportment of the as-synthesized SSQ-GO-TMEMAI-POAP film may attributed to the high surface area, accessible pores, good electron transferring and prevented resistance. Besides, the reversible operation, great columbic competence, and a typical capacitor achievement of specimens can be achieved from the identical periods of charging and discharging [74]. Furthermore, equilateral triangle shapes for SSQ-GO-TMEMAI-POAP electrode recommends an ideal capacitive performance and excellent reversibility throughout the GCD operations. This may attribute to the uniform distribution of POAP and ionic liquids on the SSQ-GO-TMEMAI-POAP, resulting in recovered electrical conductivity and active redox reactions. Fig. 8b-d indicates the GCD plots when SSQ-POAP, SSQ-GO-POAP, and SSQ-GO-TMEMAI-POAP employed as electrode at different current densities between 1 and 16 A g^{-1}. Fig. 8.e exhibits the estimated specific capacitance as a function of discharge current density ranged from 1 to 16 A g^{-1}. Actually, by increasing the values of the current density, the related capacitances go down. At the current density of 1 A g^{-1}, the specific capacitance of SSQ-POAP, SSQ-GO-POAP, and SSQ-GO-TMEMAI-POAP electrodes touched the measures of 368, 501, and 649 F g^{-1}, and then hit the points of 208, 304, and 448 F g^{-1} (43, 39 and 30% capacitance loss) at 16 A g^{-1}, respectively. These outcomes expose the reality of higher convenient and appropriate electroactive sites in SSQ-GO-TMEMAI-POAP electrode as opposed to its contestants.

The assessed capacitance retention was plotted against the number of cycles shown in Fig. 8f-h at the current density of 16 A g^{-1}. By rising the number of cycles, the specific capacitance clearly falls, after 4000 cycles, the estimated capacitance touched the values of 89.3 and 92.6% for SSQ-POAP, SSQ-GO-POAP, respectively. the retention capacitance of SSQ-GO-TMEMAI-POAP observed at about 95% during 500 periods and stayed at this point for the rest of the periods. It can be concluded that the presence of graphene oxide with its functional groups can significantly increase the electrochemical stability of the samples. Concerning the ionic liquid containing sample of SSQ-GO-TMEMAI-POAP, the electrochemical stability was clearly improved, so that in the primary cycles after a drop of almost 6% (within 500 cycles), the measured capacitance stayed unchanged for the rest of the cycles.

Totally, the notable growth in electrochemical performance of the SSQ-GO-TMEMAI-POAP can be associated with electrode activation which can raise the number of available electroactive sites and increase electrolyte accessibility, as well as the existence of the IL molecule on the functionalized GO surface that holds more beneficial supercapacitive performance than that of SSQ-POAP.

Besides, the preferences of specific capacitance values and cycling stability calculated through the GCD for all as-prepared electrodes are in striking agreement with the CV measurements. Among SSQ-containing samples, chiefly those united with conductive polymers, ionic liquids, and functional graphene oxide SSQ-GO-TMEMAI-POAP showed the most desirable capacitance performance and cyclic stability [75–78]. The electrochemical performance of the as-synthesized electrode and a list of materials that were successfully employed in SC devices are summarized in Table 1. Based on the provided data, the SSQ-GO-TMEMAI-POAP compared to the reported composites have a promising output which enables it towards high recommended supercapacitor designs.

The further electrochemical analysis was carried out using EIS as a promising non-constructive technique to study the employed samples in supercapacitors. The Nyquist plots of the device including a Faradaic impedance in parallel with a constant phase element (CPE) can be fitted based on modified Randle equivalent circuit represented in Fig. 9. At low frequencies the ion diffusion at interfaces of the electrolyte-electrode originates the spike region (Warburg region). Additionally, the Faradaic impedance is a combination of Warburg impedance (Z_W) attributed to the diffusion or mass-controlled processes while charge transfer resistance (R_{ct}) is due to kinetically controlled procedures and an interaction between the ions of electrolyte and redox-active electrode material in the high-frequency areas [92,93]. Both SSQ-GO-TMEMAI-POAP and SSQ-GO-POAP electrodes possess adequate R_{ct} states and reliable electrical conductivities toward functional supercapacitor utilizations. Moreover, the capacitive behavior in the high-frequency areas may be assigned to the aforementioned charge transfer mechanism [94]. Furthermore, Nyquist plots manifest patterns of a vertical line to the imaginary part Z″ axis (roughly identical to Z″ axis) as a function of the real part (Z′) of the impedance over low-frequency wards. Based on the mentioned comments, it can be supposed that the SSQ-GO-TMEMAI-POAP electrode had an ideal pseudocapacitive nature in low-frequency domains [89,95,96]. The EIS evaluations were managed at the frequency sweep ranged in 100 kHz 0.01 Hz at a potential of about 0 V with an alternate domain voltage of 5 mV. EIS figures can be adapted via the equivalent circuit consisting of a charge transfer R_{ct}, bulk solution resistance R_s, a pseudocapacitive component C_p from redox process of the electroactive groups in GO surface, and a constant phase element (CPE) applied as a double-layer capacitance (C_{dl}), CF denotes the pseudocapacitance of the electrode. And also, Z_W (Warburg impedance) originating from a diffusion-controlled process at low-frequency. Table 2 describes the measured values of R_S, CPE, R_{ct}, Z_W, and CF, after fitting process. Concerning the SSQ-POAP, SSQ-GO-POAP, and SSQ-GO-TMEMAI-POAP, the R_S and R_{ct} were obtained

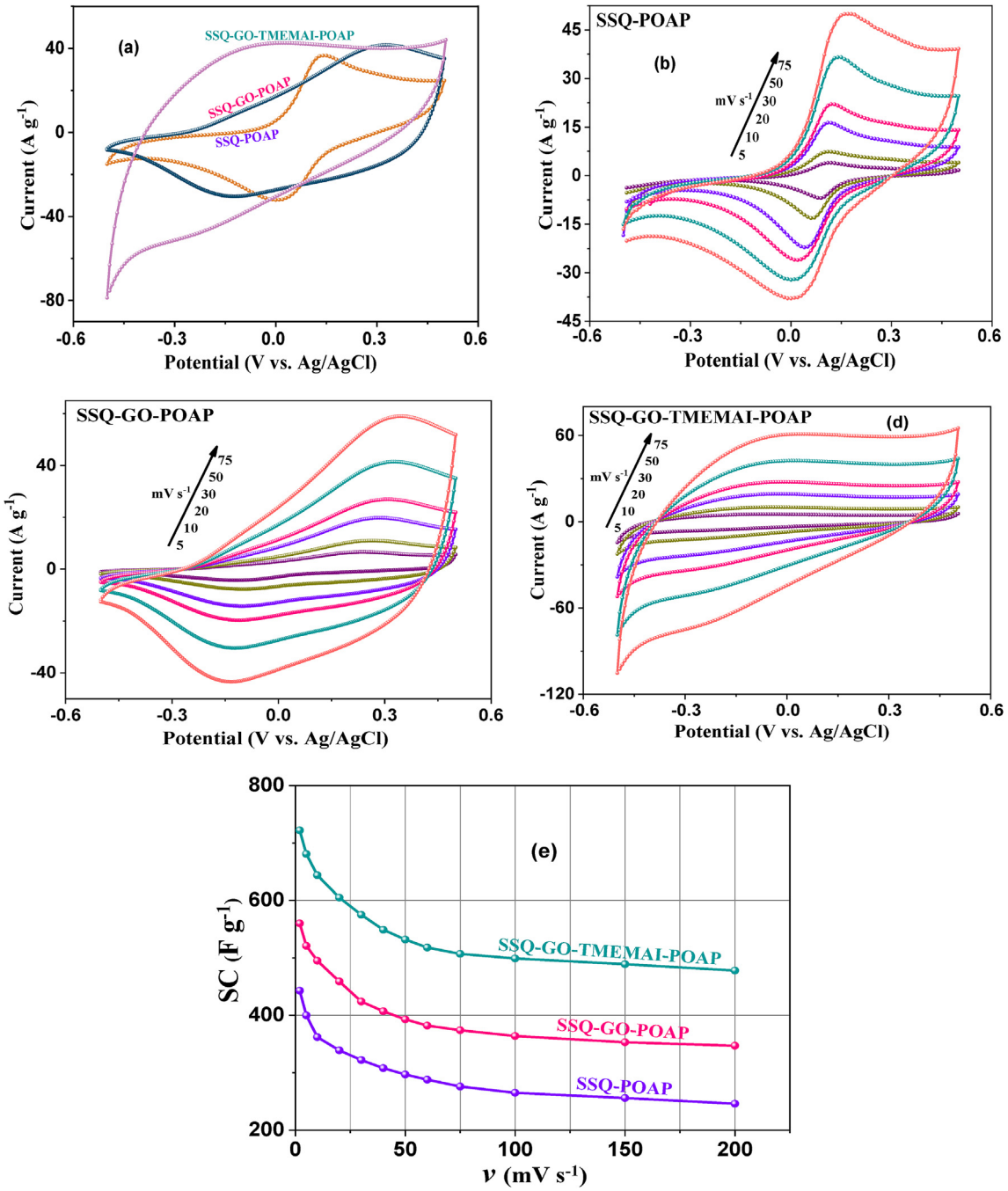

Fig. 7. Three-electrode tests: (a) The stacked CV diagrams of SSQ-POAP, SSQ-GO-POAP, and SSQ-GO-TMEMAI-POAP, CV diagrams at different scan rate ranged from 5 to 75 mV s^{-1} for (b) SSQ-POAP, (c) SSQ-GO-POAP, and (d) SSQ-GO-TMEMAI-POAP. (d) Calculated specific capacitance during the different sweep rate within 5–200 mV s^{-1}.

as (0.79 Ω, 0.9 Ω), (0.78 Ω, 0.65 Ω) and (0.78 Ω, 0.55 Ω), respectively. The outcomes comprehensibly express the significantly reduced R_{ct} of the SSQ-GO-TMEMAI-POAP composite compared with the other competitors. Z_W attributes to the Warburg resistance resided in the lower frequency appeared as straight edges. These straightforward lines ordinarily are a manifestation of the higher fluctuations in ion diffusion pathway dimensions and a provide a barrier to ion mobility which is not good for SC applications [97,98]. As can be seen in Fig. 9, the SSQ-POAP electrode has a higher Warburg resistance compared to the counterparts, while the SSQ-GO-TMEMAI-POAP indicates the shortest line and is more inclined to a perpendicular line, making an evidence of easier electron transfer ad efficient diffusion path. The evaluated values of R_S, Z_W, CPE, CF, and R_{ct} are listed in Table 2 for the SSQ-GO-TMEMAI-POAP electrode confirming an improved electrochemical performance compared to two other electrodes.

6. Electrochemical performances of the SSQ-GO-TMEMAI-POAP//SSQ-GO-TMEMAI-POAP SSC devices

To study the electrochemical performance of the SSQ-GO-TMEMAI-POAP, this nanocomposite was used in negative and positive electrodes in symmetric supercapacitor (SSC) device. The SSQ-GO-TMEMAI-POAP is acknowledged as an excellent faradaic

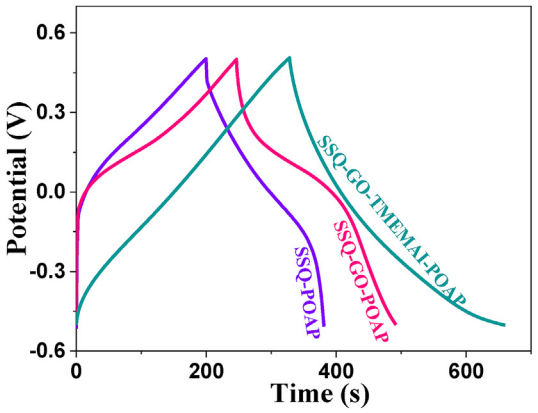
Potential (V)
Time (s)
SSQ-GO-TMEMAI-POAP
SSQ-GO-POAP
SSQ-POAP

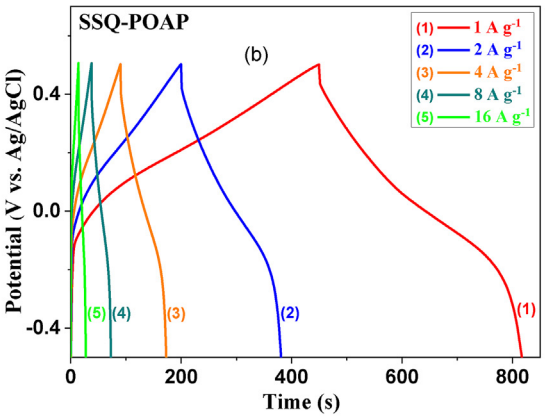
SSQ-POAP
(b)
(1) 1 A g-1
(2) 2 A g-1
(3) 4 A g-1
(4) 8 A g-1
(5) 16 A g-1
Potential (V vs. Ag/AgCl)
Time (s)

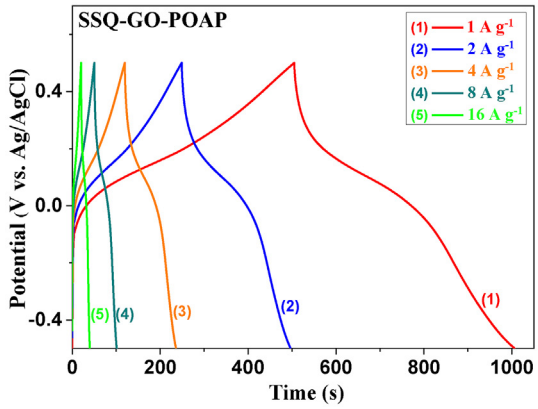
SSQ-GO-POAP
(1) 1 A g-1
(2) 2 A g-1
(3) 4 A g-1
(4) 8 A g-1
(5) 16 A g-1
Potential (V vs. Ag/AgCl)
Time (s)

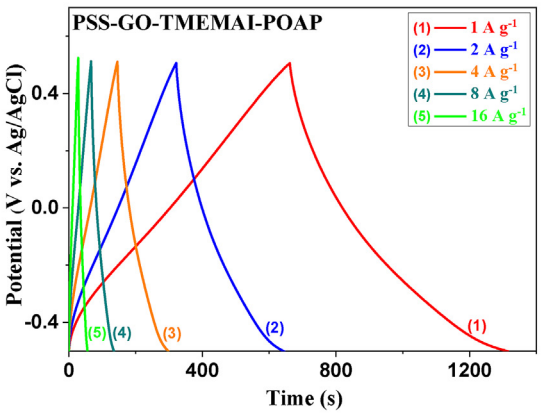
PSS-GO-TMEMAI-POAP
(1) 1 A g-1
(2) 2 A g-1
(3) 4 A g-1
(4) 8 A g-1
(5) 16 A g-1
Potential (V vs. Ag/AgCl)
Time (s)

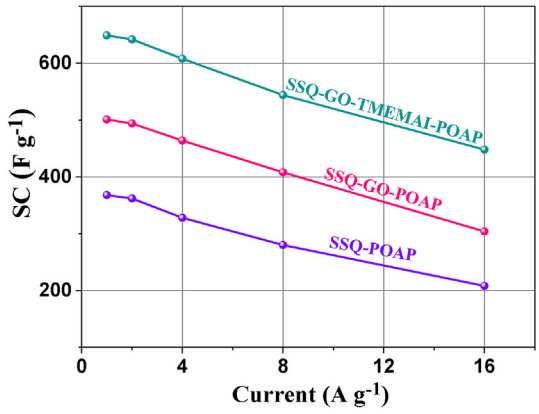
SC (F g-1)
Current (A g-1)
SSQ-GO-TMEMAI-POAP
SSQ-GO-POAP
SSQ-POAP

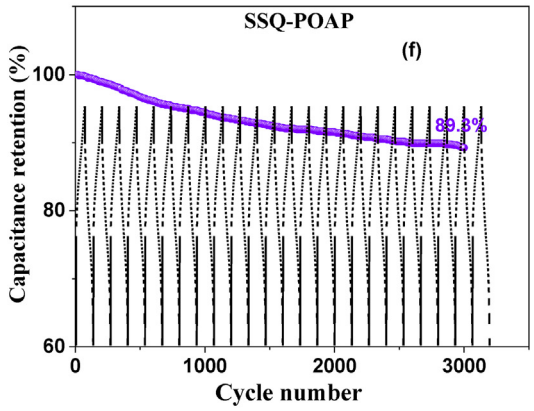
SSQ-POAP
(f)
89.3%
Capacitance retention (%)
Cycle number

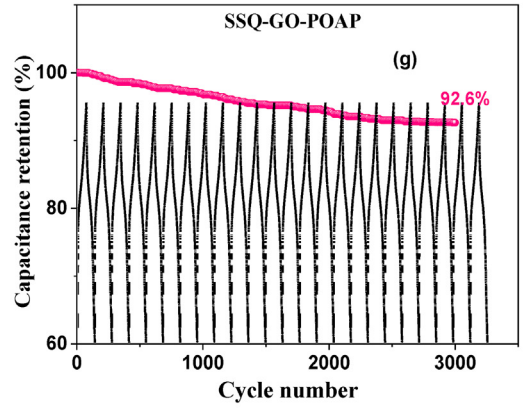
SSQ-GO-POAP
(g)
92.6%
Capacitance retention (%)
Cycle number

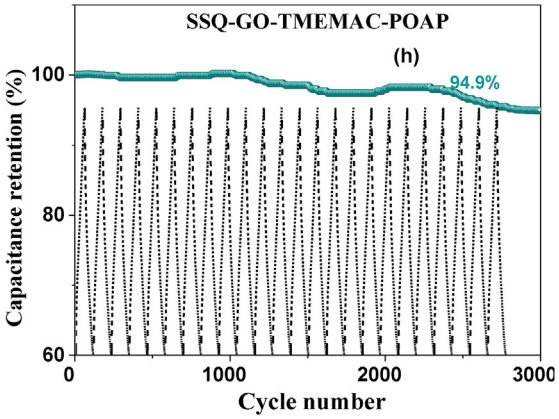
SSQ-GO-TMEMAC-POAP
(h)
94.9%
Capacitance retention (%)
Cycle number

Table 1
Comparison of electrochemical Behavior of between SSQ-GO-TMEMAI-POAP and a Couple of Reported Electrode Materials.

Sample	Electrolyte	Specific Capacitance	Measurement Condition	Cycling Stability	Ref.
C–Fe/PANI/Ni-GF	1 M $NaNO_3$	139.9 F g^{-1}	1 A g^{-1}	91%, 10,000 cycles (5 A g^{-1})	[79]
Magnetite (Fe3O4)/carbon black	0.5 M Na2SO4	282 F g^{-1}	3 A g^{-1}	98.5%, 10,000 cycles	[80]
PANI NWA/3D HGBs	1 M H_2SO_4	643 F g^{-1}	1 A g^{-1}	89%, 5000 cycles	[81]
rGO/PDA/NF	1 M Na_2SO_4	566.9 F g^{-1}	1 A g^{-1}	77.9%, 2000 cycles	[82]
S-graphene//S-graphene	BMIM-PF_6	150 F g^{-1}	2 A g^{-1}	95%, 20,000 cycles (2 A g^{-1})	[83]
Fe3O4/rGO	1 M KOH	220.1 F g^{-1}	0.5 A g^{-1}	remains stable after 3000 cycles	[76]
PHRGs	6 M KOH	284.1 F g^{-1}	0.3 A g^{-1}	88%, 10,000 cycles	[84]
SNG-H	6 M KOH	233.4 F g^{-1}	1 A g^{-1}	95.1%, 5000 cycles	[85]
quasi-cubic Fe3O4/rGO	6 M KOH	216.7 F g^{-1}	0.5 A g^{-1}	73.2%, 3000 cycles	[86]
NCG	6 M KOH	225.0 F g^{-1}	0.5 A g^{-1}	96.8%, 10,000 cycles (10 A g^{-1})	[87]
RG	1 M H_2SO_4	245 F g^{-1}	1 A g^{-1}	85.8%, 5000 cycles	[88]
rGO/Fe3O4/PANI	1 M H2SO4	486.5 F g^{-1}	1 A g^{-1}	52.1%, 2000 cycles	[89]
APRG-30	6 M KOH	260.2 F g^{-1}	0.3 A g^{-1}	88.4%, 10,000 cycles	[90]
PANI/VG/Ti	0.5 M H_2SO_4	535.7 F g^{-1} 461.2 F g^{-1}	40 A g^{-1} 50 mV s^{-1}	86%, 10,000 cycles	[91]
SSQ-GO-TMEMAI-POAP	3 M KOH	649 F g^{-1}	1 A g^{-1}	~95%, 4000 cycles (16 A g^{-1})	This work

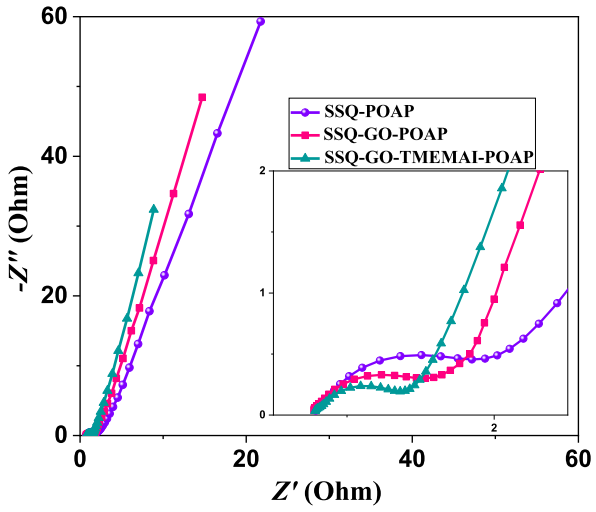

Fig. 9. The Nyquist plot for SSQ-POAP, SSQ-GO-POAP, and SSQ-GO-TMEMAI-POAP.

Table 2
Evaluated values of R_S, Z_W, CPE, CF, and R_{ct}, through CNLS fitting of the experimental impedance spectra rely on the recommended equivalent circuit.

	SSQ-POAP	SSQ-GO-POAP	SSQ-GO-TMEMAI-POAP
R_s	0.79	0.78	0.78
R_{ct}	0.9	0.68	0.55
Q_1 (mF)	0.0028	0.0031	0.0045
N	0.84	0.82	0.8
W	0.22	0.29	0.41
CF (mF)	0.37001	0.42795	0.48148

electrode because it owns a large surface area and the expanded CV diagrams during the −0.5 to 0.5 V. This composite was exhibited the faradaic behaviors of the electrode (with a good stable potential window which represents a capacitive characteristic. Accordingly, the CVs of SSQ-GO-TMEMAI-POAP//SSQ-GO-TMEMAI-POAP SSC device was considered and the CV curves are shown in Fig. 10.a. Concerning the CV measurements, all CV curves of the as-designed symmetric system keep the same patterns in KOH (3 M) during the scan rates ranged from 5 to 100 mV s^{-1}. By altering the rates of potential applied, the specific capacitance was measured for each scan rate, where the Fig. 10 b shows the obtained capacitance versus its scan rates for that symmetric device.

The electrochemical test for two electrode system was followed by recording the GCD curves of the SSQ-GO-TMEMAI-POAP//SSQ-GO-TMEMAI-POAP device displayed in Fig. 10.c. These diagrams exhibit reasonably symmetric frames when examined in multiple current densities. Besides, the diagram of specific capacitance was plotted against the current density indicated in Fig. 10.d. The high specific capacitance of 450 F g^{-1} was observed for the cells containing SSQ-GO-TMEMAI-POAP//SSQ-GO-TMEMAI-POAP at the current density of 0.5 A g^{-1}, while it dropped with an almost constant slope to touch the capacitance of 323, at the current density of 16 A g^{-1}. During this evaluation, approximately 72% of initial capacitance was retained showing a good capacitive achievement for the employed SSQ-GO-TMEMAI-POAP electrodes.

The retention capacitance within consecutive cycles is an indication of electrochemical stability of two-electrode SSQ-GO-TMEMAI-POAP//SSQ-GO-TMEMAI-POAP system shown in Fig. 10.e, when after 3000 charge-discharge periods approximately only 4% of the initial capacitance was lost at the current density of 16 A g^{-1}. With a closer look at the diagram, the remaining capacity firstly experienced an upward trend due to the available more electroactive sites and activation processes in which the trapped cations gradually diffused out, and this slope continued for periods close to 900 cycles. Almost halfway through the cycle, the capacity pattern experienced a decreasing trend and remained constant at 96%, showing an outstanding electrochemical stability [99–101].

Power density and energy density accounted as critical determinants to move forward from the laboratory scale into the practical application of the SSC devices in manufacturing scale. To compare the various energy delivery capability options, a very frequently used diagram of Ragone plot (developed by David V. Ragone) [15,102–104] is plotted in log-log scale shown in Fig. 10.f, where both energy and power densities ascribed in vertical and horizontal axis, respectively. It shows that graphene oxide with wide potential window and high conductivity when blended with ionic liquid and conductive polymer in the presence of cubic

Fig. 8. Three electrode measurements: (a) GCD plots of SSQ-POAP, SSQ-GO-POAP, SSQ-GO-TMEMAI-POAP at 2 A g^{-1}. GCD plots of (b) SSQ-POAP, (c) SSQ-GO-POAP, and (d) SSQ-GO-TMEMAI-POAP at different current densities. (e) Specific capacitance at different current densities (1–16 A g^{-1}). Capacitance retention during 3000 cycles for (f) SSQ-POAP, (g) SSQ-GO-POAP, and (h) SSQ-GO-TMEMAI-POAP electrodes.

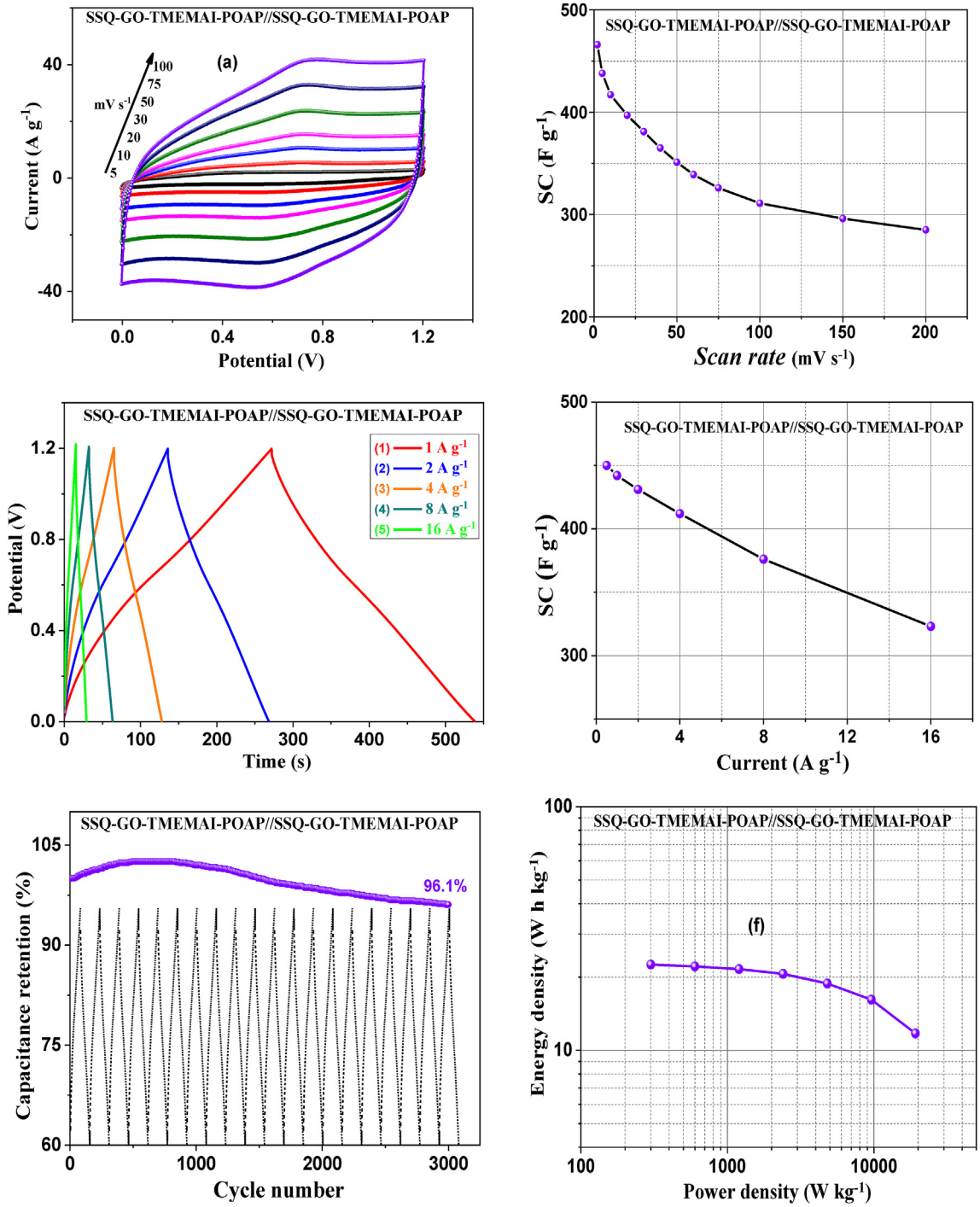

Fig. 10. Electrochemical tests for SSQ-GO-TMEMAI electrode, (a) CV at different scan rate from 5 to 100 mV s^{-1}, (b) specific capacitance at different scan rates from 5 to 100 mV s^{-1}, (c) GCD diagram at different current densities from 1 to 16 A g^{-1}, (d) Specific capacitance against different current densities from 1 to 16 A g^{-1}, (e) Retention capacity during 3000 Cycles, and (f) Ragone plot with evaluating Energy density at power density.

structure of SSQ, can improve the electrochemistry of redox reactions in pseudocapacitive mechanism to deliver higher available energy where large power originated. Compared to the reported symmetric devices including V_2O_5/MWCNTs (62 Wh kg^{-1}, 11.5 W kg^{-1}) [105], PyHCP-800/PANI (3.72 Wh kg^{-1}, 65.07 W kg^{-1}) [106], MnSe@CT (55.42 Wh kg^{-1}, 894.25 W kg^{-1}) [107], $BiFeO_3$-RGO (18.62 W h kg^{-1} at 950 W kg^{-1}) [108], Fe_3O_4/graphene (9 W h kg^{-1} at 3000 W kg^{-1}) [109], GP/SWNTs/PPy (28.8 Wh kg^{-1}, 1975.22 W kg^{-1}) [110], Boron-doped graphene aerogels (B-GAs) (12.65 Wh kg^{-1}, 150 W kg^{-1}) [111], 3D HGBs (26.4 Wh kg^{-1}, 563.5 W kg^{-1}) [81], PANI NWA/3D HGBs (26.4 Wh kg^{-1}, 563.5 W kg^{-1}) [81], S-doped graphene (in $EMIMBF_4$) (4.4 Wh kg^{-1}, 495 W kg^{-1}) [112], and oxygen-enriched crumpled graphene (OCGN) (20.4 Wh kg^{-1}, 450 W kg^{-1}) [113], the as-designed symmetric SSQ-GO-TMEMAI-POAP//SSQ-GO-TMEMAI-POAP system, showed energy density (Wh kg^{-1}) at power density (W kg^{-1}) as following arrays (22.5 Wh kg^{-1}, 300 W kg^{-1}), (22.1 Wh kg^{-1}, 600 W kg^{-1}), (21.55 Wh kg^{-1}, 1200 W kg^{-1}), (20.6 Wh kg^{-1},

2400 W kg^{-1}), (18.8 Wh kg^{-1}, 4800 W kg^{-1}), (16.15 Wh kg^{-1}, 9600 W kg^{-1}) and (11.73 Wh kg^{-1}, 19,200 W kg^{-1}). It shows that the provided energy delivery at power density is really improved towards supercapacitor applications.

7. Conclusion

To summarize the current investigation, we firstly synthesized a functional graphene oxide including SSQ molecules with porous structure as SSQ-GO that characterized by XPS, XRD, SEM, EDX techniques and Rietveld Jacobian simulation. The porous structure of SSQ-GO composited by conductive ionic liquid TMEMAI and POAP coated on it through electro-synthesis method to employ as an electrode in a three-electrode system. Among the as-prepared SSQ-GO-POAP, TMEMAI-POAP, and SSQ-GO-TMEMAI-POAP, the last composite represented high specific capacitance in three-electrode and two-electrode system as 722 F g^{-1} at 5 mV s^{-1} and 450 F g^{-1} at 0.5 A g^{-1}, respectively. Besides, the SSQ-GO-TMEMAI-POAP showed an improved conductivity, good cycle life and durability (95% @ 3000 Cycles). The fractal concept showed a porous structure by plotting current-potential diagram and energy density enhanced. Based on the EIS analysis and Nyquist diagram, the resistance of the bulk and R_{ct} were decreased accompanied with short and close to vertical line, indicating an appropriate supercapacitor behavior resulting in high conductivity. This investigation opens a new insight into the preparing high-efficient pseudocapacitive electrode materials with synergic electrochemical effects from functional graphene oxide, ionic liquid and conductive polymer towards developing high-performance energy storage systems.

Declaration of competing interest

None.

Acknowledgement

The authors would like to gratefully thank the Research Affairs Division at the Lloyd's Register Foundation, UK for the financial support.

Appendix A. Supplementary data

Supplementary data to this article can be found online at https://doi.org/10.1016/j.electacta.2020.136663.

References

[1] D.D.L. Chung, Development, design and applications of structural capacitors, Appl. Energy 231 (2018) 89–101, https://doi.org/10.1016/j.apenergy.2018.09.132.
[2] Z. Zhang, F. Xiao, L. Qian, J. Xiao, S. Wang, Y. Liu, Facile synthesis of 3D MnO2–graphene and carbon nanotube–graphene composite networks for high-performance, flexible, all-solid-state asymmetric supercapacitors, Adv. Energy Mater. 4 (2014) 1400064.
[3] K. Chen, Q. Wang, Z. Niu, J. Chen, Graphene-based materials for flexible energy storage devices, J. Energy Chem. 27 (2018) 12–24, https://doi.org/10.1016/j.jechem.2017.08.015.
[4] Z. Liu, H. Zhang, Q. Yang, Y. Chen, Graphene/V2O5 hybrid electrode for an asymmetric supercapacitor with high energy density in an organic electrolyte, Electrochim. Acta 287 (2018) 149–157, https://doi.org/10.1016/j.electacta.2018.04.212.
[5] D.J. Ahirrao, K. Mohanapriya, N. Jha, V2O5 nanowires-graphene composite as an outstanding electrode material for high electrochemical performance and long-cycle-life supercapacitor, Mater. Res. Bull. 108 (2018) 73–82, https://doi.org/10.1016/j.materresbull.2018.08.028.
[6] Y. Liu, M. Yao, L. Zhang, Z. Niu, Large-scale fabrication of reduced graphene oxide-sulfur composite films for flexible lithium-sulfur batteries, J. Energy Chem. 38 (2019) 199–206, https://doi.org/10.1016/j.jechem.2019.03.034.
[7] S. Zheng, Y. Fu, L. Zheng, Z. Zhu, J. Chen, Z. Niu, D. Yang, PEDOT-engineered Bi 2 O 3 nanosheet arrays for flexible asymmetric supercapacitors with boosted energy density, J. Mater. Chem. A. 7 (2019) 5530–5538, https://doi.org/10.1039/c9ta00854c.
[8] H. Cao, N. Wu, Y. Liu, S. Wang, W. Du, J. Liu, Facile synthesis of rod-like manganese molybdate crystallines with two-dimensional nanoflakes for supercapacitor application, Electrochim. Acta 225 (2017) 605–613, https://doi.org/10.1016/j.electacta.2017.01.021.
[9] R. Wang, Q.-R. Wang, M.-J. Yao, K.-N. Chen, X.-Y. Wang, L.-L. Liu, Z.-Q. Niu, J. Chen, Flexible ultrathin all-solid-state supercapacitors, Rare Met. 37 (2018) 536–542, https://doi.org/10.1007/s12598-018-1034-x.
[10] Y. Liu, S. Li, Y. Wang, J. Yang, A template-free synthesis of porous 3D honeycomb-like carbons for supercapacitor electrodes, J. Mater. Sci. Mater. Electron. 30 (2019) 5744–5752, https://doi.org/10.1007/s10854-019-00869-1.
[11] K. Mohanapriya, D.J. Ahirrao, N. Jha, Highly crumpled solar reduced graphene oxide electrode for supercapacitor application, in: D A, S S, B A (Eds.), 62nd DAE Solid State Phys. Symp. 2017, American Institute of Physics Inc., Department of Physics, Institute of Chemical Technology, Nathalal Parekh Marg, Matunga East, Mumbai, 2018, https://doi.org/10.1063/1.5028759, 400019, India.
[12] Q. Chang, L. Li, L. Sai, W. Shi, Q. Chen, L. Huang, Interconnected binary carbon hybrids for supercapacitor electrode, Electrochim. Acta 251 (2017) 293–300, https://doi.org/10.1016/j.electacta.2017.08.109.
[13] C.-H. Mun, C.V.V.M. Gopi, R. Vinodh, S. Sambasivam, I.M. Obaidat, H.-J. Kim, Microflower-like nickel sulfide-lead sulfide hierarchical composites as binder-free electrodes for high-performance supercapacitors, J. Energy Storage. 26 (2019) 100925.
[14] Y. Wang, Y. Liu, W. Liu, G. Zhang, G. Liu, H. Chen, J. Yang, Large-scale synthesis of highly porous carbon nanosheets for supercapacitor electrodes, J. Alloys Compd. 677 (2016) 105–111, https://doi.org/10.1016/j.jallcom.2016.03.232.
[15] Y. Shabangoli, M.S. Rahmanifar, M.F. El-Kady, A. Noori, M.F. Mousavi, R.B. Kaner, Thionine functionalized 3D graphene aerogel: combining simplicity and efficiency in fabrication of a metal-free redox supercapacitor, Adv. Energy Mater. 8 (2018), https://doi.org/10.1002/aenm.201802869.
[16] K. Mohanapriya, N. Jha, Simple and low cost production of wrinkled graphene - Carbon particles composite for supercapacitor application, in: M S K B, B S B R (Eds.), 5th Int. Conf. Adv. Energy Res. ICAER 2015, Elsevier Ltd, Department of Chemical Engineering, Institute of Chemical Technology, Matunga, Mumbai, 2018, pp. 23,326–23332, https://doi.org/10.1016/j.matpr.2018.11.069, 400,019, India.
[17] G.M. Tomboc, H. Kim, Derivation of both EDLC and pseudocapacitance characteristics based on synergistic mixture of NiCo2O4 and hollow carbon nanofiber: an efficient electrode towards high energy density supercapacitor, Electrochim. Acta 318 (2019) 392–404, https://doi.org/10.1016/j.electacta.2019.06.112.
[18] Y. Wang, Y. Chen, Y. Liu, W. Liu, P. Zhao, Y. Li, Y. Dong, H. Wang, J. Yang, Urchin-like Ni1/3Co2/3(CO3)0.5OH·0.11H2O anchoring on polypyrrole nanotubes for supercapacitor electrodes, Electrochim. Acta 295 (2019) 989–996, https://doi.org/10.1016/j.electacta.2018.11.116.
[19] C.Y. Foo, A. Sumboja, D.J.H. Tan, J. Wang, P.S. Lee, Flexible and highly scalable V2O5-rGO electrodes in an organic electrolyte for supercapacitor devices, Adv. Energy Mater. 4 (2014) 1400236.
[20] K.V.G. Raghavendra, C.V.V.M. Gopi, R. Vinodh, S.S. Rao, I.M. Obaidat, H.-J. Kim, Facile synthesis of nanoparticles anchored on honeycomb-like MnCo2S4 nanostructures as a binder-free electroactive material for supercapacitors, J. Energy Storage. 27 (2020), https://doi.org/10.1016/j.est.2019.101159.
[21] T. Anitha, A.E. Reddy, Y.A. Kumar, Y.-R. Cho, H.-J. Kim, Erratum: one-step synthesis and electrochemical performance of a PbMoO4/CdMoO4 composite as an electrode material for high-performance supercapacitor applications, Dalton Trans. 48 (2019) 10652–10660, https://doi.org/10.1039/C9DT01931F. Dalt. Trans. 49 (2020) 941. doi:10.1039/c9dt90290b.
[22] L. Jiang, L. Sheng, C. Long, T. Wei, Z. Fan, Functional pillared graphene frameworks for ultrahigh volumetric performance supercapacitors, Adv. Energy Mater. 5 (2015) 1500771.
[23] C.H. Ng, H.N. Lim, Y.S. Lim, W.K. Chee, N.M. Huang, Fabrication of flexible polypyrrole/graphene oxide/manganese oxide supercapacitor, Int. J. Energy Res. 39 (2015) 344–355.
[24] X. Liu, Y. Zheng, X. Wang, Controllable preparation of polyaniline–graphene nanocomposites using functionalized graphene for supercapacitor electrodes, Chem. Eur J. 21 (2015) 10408–10415.
[25] Z. Weng, Y. Su, D. Wang, F. Li, J. Du, H. Cheng, Graphene–cellulose paper flexible supercapacitors, Adv. Energy Mater. 1 (2011) 917–922, https://doi.org/10.1002/aenm.201100312.
[26] D.H. Seo, Z.J. Han, S. Kumar, K.(Ken, Structure-Controlled Ostrikov, Vertical graphene-based, binder-free electrodes from plasma-reformed butter enhance supercapacitor performance, Adv. Energy Mater. 3 (2013) 1316–1323, https://doi.org/10.1002/aenm.201300431.
[27] Y. Xu, M.G. Schwab, A.J. Strudwick, I. Hennig, X. Feng, Z. Wu, K. Müllen, Screen-printable thin film supercapacitor device utilizing graphene/polyaniline inks, Adv. Energy Mater. 3 (2013) 1035–1040, https://doi.org/10.1002/aenm.201300184.
[28] L.J. Wang, M.F. El-Kady, S. Dubin, J.Y. Hwang, Y. Shao, K. Marsh, B. McVerry, M.D. Kowal, M.F. Mousavi, R.B. Kaner, Flash converted graphene for ultrahigh power supercapacitors, Adv. Energy Mater. 5 (2015), https://doi.org/

10.1002/aenm.201500786.
[29] J. Chen, X. Wang, J. Wang, P.S. Lee, Sulfidation of NiMn-layered double hydroxides/graphene oxide composites toward supercapacitor electrodes with enhanced performance, Adv. Energy Mater. 6 (2015), https://doi.org/10.1002/aenm.201501745.
[30] G.A. Snook, P. Kao, A.S. Best, Conducting-polymer-based supercapacitor devices and electrodes, J. Power Sources 196 (2011) 1–12.
[31] S.-Y. Hsu, S.-C. Lin, J.-A. Wang, C.-C. Hu, C.-C.M. Ma, D.-H. Tsai, Aerosol-based synthesis of silsesquioxane-graphene oxide and graphene-manganese oxide nanocomposites for high-performance asymmetric supercapacitors, Electrochim. Acta 296 (2019) 427–437, https://doi.org/10.1016/j.electacta.2018.11.065.
[32] H. Zhang, X. Deng, H. Huang, G. Li, X. Liang, W. Zhou, J. Guo, W. Wei, S. Tang, Hetero-structure arrays of NiCoO2 nanoflakes@nanowires on 3D graphene/nickel foam for high-performance supercapacitors, Electrochim. Acta 289 (2018) 193–203, https://doi.org/10.1016/j.electacta.2018.08.071.
[33] E. Kowsari, Ionic Liquids for Green Energy Applications, Nova Science Publishers, 2018.
[34] B. Qiu, B. Lin, F. Yan, Ionic liquid/poly(ionic liquid)-based electrolytes for energy devices, Polym. Int. 62 (2013) 335–337, https://doi.org/10.1002/pi.4454.
[35] X. Zhang, M. Kar, T.C. Mendes, Y. Wu, D.R. MacFarlane, Supported ionic liquid gel membrane electrolytes for flexible supercapacitors, Adv. Energy Mater. 8 (2018), https://doi.org/10.1002/aenm.201702702.
[36] A. Ehsani, E. Kowsari, F. Boorboor Ajdari, R. Safari, H. Mohammad Shiri, Influence of newly synthesized geminal dicationic ionic liquid on electrochemical and pseudocapacitance performance of conductive polymer electroactive film, J. Colloid Interface Sci. 505 (2017) 1158–1164, https://doi.org/10.1016/j.jcis.2017.07.001.
[37] A. Ehsani, E. Kowsari, F. Boorboorajdari, H.M. Shiri, Enhanced pseudocapacitance performance of conductive polymer electroactive film in the presence of green compound of 1-Butyl-3-methylimidazolium Chloride: electrochemical and DFT study, J. Colloid Interface Sci. (2017), https://doi.org/10.1016/j.jcis.2017.10.046.
[38] R. Yan, M. Antonietti, M. Oschatz, Toward the experimental understanding of the energy storage mechanism and ion dynamics in ionic liquid based supercapacitors, Adv. Energy Mater. 8 (2018), https://doi.org/10.1002/aenm.201800026.
[39] F. Boorboor Ajdari, E. Kowsari, A. Ehsani, P-type conductive polymer/zeolitic imidazolate framework-67 (ZIF-67) nanocomposite film: synthesis, characterization, and electrochemical performance as efficient electrode materials in pseudocapacitors, J. Colloid Interface Sci. 509 (2018) 189–194, https://doi.org/10.1016/j.jcis.2017.08.098.
[40] L.-Q. Fan, Q.-M. Tu, C.-L. Geng, J.-L. Huang, Y. Gu, J.-M. Lin, Y.-F. Huang, J.-H. Wu, High energy density and low self-discharge of a quasi-solid-state supercapacitor with carbon nanotubes incorporated redox-active ionic liquid-based gel polymer electrolyte, Electrochim. Acta 331 (2020) 135425, https://doi.org/10.1016/j.electacta.2019.135425.
[41] F. Poli, D. Momodu, G.E. Spina, A. Terella, B.K. Mutuma, M.L. Focarete, N. Manyala, F. Soavi, Pullulan-ionic liquid-based supercapacitor: a novel, smart combination of components for an easy-to-dispose device, Electrochim. Acta 338 (2020) 135872, https://doi.org/10.1016/j.electacta.2020.135872.
[42] Q. Zheng, A. Kvit, Z. Cai, Z. Ma, S. Gong, A freestanding cellulose nanofibril–reduced graphene oxide–molybdenum oxynitride aerogel film electrode for all-solid-state supercapacitors with ultrahigh energy density, J. Mater. Chem. A. 5 (2017) 12528–12541, https://doi.org/10.1039/C7TA03093B.
[43] F.B. Ajdari, E. Kowsari, A. Ehsani, M. Schorowski, T. Ameri, New synthesized ionic liquid functionalized graphene oxide: synthesis, characterization and its nanocomposite with conjugated polymer as effective electrode materials in an energy storage device, Electrochim. Acta 292 (2018) 789–804.
[44] A. Ehsani, E. Kowsari, F.B. Ajdari, R. Safari, H.M. Shiri, Sulfonated graphene oxide and its nanocomposites with electroactive conjugated polymer as effective pseudocapacitor electrode materials, J. Colloid Interface Sci. 497 (2017) 258–265.
[45] F.B. Ajdari, E. Kowsari, A. Ehsani, Ternary nanocomposites of conductive polymer/functionalized GO/MOFs: synthesis, characterization and electrochemical performance as effective electrode materials in pseudocapacitors, J. Solid State Chem. 265 (2018) 155–166, https://doi.org/10.1016/j.jssc.2018.05.038.
[46] F.B. Ajdari, E. Kowsari, A. Ehsani, L. Chepyga, M. Schirowski, S. Jäger, O. Kasian, F. Hauke, T. Ameri, Melamine-functionalized graphene oxide: synthesis, characterization and considering as pseudocapacitor electrode material with intermixed POAP polymer, Appl. Surf. Sci. 459 (2018) 874–883.
[47] W.S. Hummers Jr., R.E. Offeman, Preparation of graphitic oxide, J. Am. Chem. Soc. 80 (1958) 1339.
[48] Z.W. Lu, Y.H. Wang, Z. Dai, X.P. Li, C.Y. Zhang, G.Z. Sun, C.S. Gong, X.J. Pan, W. Lan, J.Y. Zhou, E.Q. Xie, One-pot sulfur-containing ion assisted microwave synthesis of reduced graphene oxide@nano-sulfur fibrous hybrids for high-performance lithium-sulfur batteries, Electrochim. Acta 325 (2019) 134920, https://doi.org/10.1016/j.electacta.2019.134920.
[49] S. Hu, Z. Wang, Y. Gu, Y. Li, Y. Jia, Clinical available circulating tumor cell assay based on tetra(4-aminophenyl) porphyrin mediated reduced graphene oxide field effect transistor, Electrochim. Acta 313 (2019) 415–422, https://doi.org/10.1016/j.electacta.2019.05.039.
[50] M. Furquan, A.R. Khatribail, S. Vijayalakshmi, S. Mitra, Efficient conversion of sand to nano-silicon and its energetic Si-C composite anode design for high volumetric capacity lithium-ion battery, J. Power Sources 382 (2018) 56–68.
[51] A. Sohrabi, A. Dolati, M. Ghorbani, M.R. Barati, P. Stroeve, Elucidation of the structural texture of electrodeposited Ni/SiC nanocomposite coatings, J. Phys. Chem. C 116 (2012) 4105–4118, https://doi.org/10.1021/jp2095714.
[52] C. Athanasekou, A. Sapalidis, I. Katris, E. Savopoulou, K. Beltsios, T. Tsoufis, A. Kaltzoglou, P. Falaras, G. Bounos, M. Antoniou, P. Boutikos, G.E. Romanos, Mixed matrix PVDF/graphene and composite-skin PVDF/graphene oxide membranes applied in membrane distillation, Polym. Eng. Sci. 59 (2019) E262–E278, https://doi.org/10.1002/pen.24930.
[53] C.K. Chua, Z. Sofer, J. Luxa, M. Pumera, Selective nitrogen functionalization of graphene by bucherer-type reaction, Chem. Eur J. 21 (2015) 8090–8095, https://doi.org/10.1002/chem.201405748.
[54] W. Zhou, J. Chen, C. He, M. Chen, X. Xu, Q. Tian, J. Xu, C.-P. Wong, Hybridizing δ-type NaxV2O5·nH2O with graphene towards high-performance aqueous zinc-ion batteries, Electrochim. Acta 321 (2019) 134689, https://doi.org/10.1016/j.electacta.2019.134689.
[55] C. Jeganathan, T.C. Sabari Girisun, S. Vijaya, S. Anandan, Improved charge collection and photo conversion of bacteriorhodopsin sensitized solar cells coupled with reduced graphene oxide decorated one-dimensional TiO2 nanorod hybrid photoanodes, Electrochim. Acta 319 (2019) 909–921, https://doi.org/10.1016/j.electacta.2019.07.036.
[56] M. Erans, M. Jeremias, L. Zheng, J.G. Yao, J. Blamey, V. Manovic, P.S. Fennell, E.J. Anthony, Pilot testing of enhanced sorbents for calcium looping with cement production, Appl. Energy 225 (2018) 392–401, https://doi.org/10.1016/j.apenergy.2018.05.039.
[57] S. Meti, M.R. Rahman, M.I. Ahmad, K.U. Bhat, Chemical free synthesis of graphene oxide in the preparation of reduced graphene oxide-zinc oxide nanocomposite with improved photocatalytic properties, Appl. Surf. Sci. 451 (2018) 67–75.
[58] A. Sohrabi, A. Dolati, M. Ghorbani, A. Monfared, P. Stroeve, Nanomechanical properties of functionally graded composite coatings: electrodeposited nickel dispersions containing silicon micro-and nanoparticles, Mater. Chem. Phys. 121 (2010) 497–505.
[59] Y. Zang, L. Li, Q. Chu, Y. Han, H. Pu, X. Feng, H. Jin, Growth of graphene/Ge/Si heterostructure on Si(001) substrate, Mater. Lett. 205 (2017) 162–164, https://doi.org/10.1016/j.matlet.2017.06.035.
[60] Y. Chen, Y. Hu, Z. Shen, R. Chen, X. He, X. Zhang, Y. Zhang, K. Wu, Sandwich structure of graphene-protected silicon/carbon nanofibers for lithium-ion battery anodes, Electrochim. Acta 210 (2016) 53–60, https://doi.org/10.1016/j.electacta.2016.05.086.
[61] S. Kellici, J. Acord, A. Vaughn, N.P. Power, D.J. Morgan, T. Heil, S.P. Facq, G.I. Lampronti, Calixarene assisted rapid synthesis of silver-graphene nanocomposites with enhanced antibacterial activity, ACS Appl. Mater. Interfaces 8 (2016) 19038–19046, https://doi.org/10.1021/acsami.6b06052.
[62] B. Sahoo, A.K. Singh, D. Behera, Graphene oxide modified superconducting and elastic parameters of YBCO superconductor, Mater. Chem. Phys. 240 (2020) 122252, https://doi.org/10.1016/j.matchemphys.2019.122252.
[63] L. Chen, C. Batchelor-McAuley, B. Rasche, C. Johnston, N. Hindle, R.G. Compton, Surface area measurements of graphene and graphene oxide samples: dopamine adsorption as a complement or alternative to methylene blue? Appl. Mater. Today. 18 (2020) 100506, https://doi.org/10.1016/j.apmt.2019.100506.
[64] R.S. Weatherup, B.C. Bayer, R. Blume, C. Ducati, C. Baehtz, R. Schlögl, S. Hofmann, In situ characterization of alloy catalysts for low-temperature graphene growth, Nano Lett. 11 (2011) 4154–4160, https://doi.org/10.1021/nl202036y.
[65] M. Zhou, X. Li, B. Wang, Y. Zhang, J. Ning, Z. Xiao, X. Zhang, Y. Chang, L. Zhi, High-performance silicon battery anodes enabled by engineering graphene assemblies, Nano Lett. 15 (2015) 6222–6228, https://doi.org/10.1021/acs.nanolett.5b02697.
[66] H.-A. Guo, S. Jou, T.-Z. Mao, B.-R. Huang, Y.-T. Huang, H.-C. Yu, Y.-F. Hsieh, C.-C. Chen, Silicon- and oxygen-codoped graphene from polycarbosilane and its application in graphene/n-type silicon photodetectors, Appl. Surf. Sci. 464 (2019) 125–130, https://doi.org/10.1016/j.apsusc.2018.09.067.
[67] Y. Yang, H.-X. Yang, Y.-Q. Wu, H. Pu, W.-J. Meng, R.-Z. Gao, D.-L. Zhao, Graphene caging core-shell Si@Cu nanoparticles anchored on graphene sheets for lithium-ion battery anode with enhanced reversible capacity and cyclic performance, Electrochim. Acta (2020) 136037, https://doi.org/10.1016/j.electacta.2020.136037.
[68] F. ARMiJO, L.I. Canales, R. Del Rio, M.A. Del Valle, POLY-0-AMINOPHENOL obtained at high potentials BY cyclic voltammetry ON SN0 (2): F electrodes: application IN quantitative determination OF ascorbic acid, J. Chil. Chem. Soc. 54 (2009) 158–162.
[69] I. Losito, F. Palmisano, P.G. Zambonin, o-Phenylenediamine electropolymerization by cyclic voltammetry combined with electrospray ionization-ion trap mass spectrometry, Anal. Chem. 75 (2003) 4988–4995.
[70] S. Sathyamoorthi, M. Sawangphruk, A simple and practical hybrid ionic liquid/aqueous dual electrolyte configuration for safe and ion-exchange membrane-free high cell potential supercapacitor, Electrochim. Acta 305 (2019) 443–451.
[71] N. Ma, S. Kosasang, N. Phattharasupakun, M. Sawangphruk, Addition of redox

additive to ionic liquid electrolyte for high-performance electrochemical capacitors of N-doped graphene aerogel, J. Electrochem. Soc. 166 (2019) A695–A703.
[72] R. McKenna, P. Djapic, J. Weinand, W. Fichtner, G. Strbac, Assessing the implications of socioeconomic diversity for low carbon technology uptake in electrical distribution networks, Appl. Energy 210 (2018) 856–869, https://doi.org/10.1016/j.apenergy.2017.07.089.
[73] Z. Kawasaki, K. Matsuura, Does a lightning channel show a fractal? Appl. Energy 67 (2000) 147–158, https://doi.org/10.1016/S0306-2619(00)00011-8.
[74] P. Suktha, P. Chiochan, A. Krittayavathananon, S. Sarawutanukul, S. Sethuraman, M. Sawangphruk, In situ mass change and gas analysis of 3D manganese oxide/graphene aerogel for supercapacitors, RSC Adv. 9 (2019) 28569–28575.
[75] C. Wu, S. Yang, J. Cai, Q. Zhang, Y. Zhu, K. Zhang, Activated microporous carbon derived from almond shells for high energy density asymmetric supercapacitors, ACS Appl. Mater. Interfaces 8 (2016) 15288–15296.
[76] Q. Wang, L. Jiao, H. Du, Y. Wang, H. Yuan, Fe3O4 nanoparticles grown on graphene as advanced electrode materials for supercapacitors, J. Power Sources 245 (2014) 101–106.
[77] S. Kalasina, N. Phattharasupakun, T. Maihom, V. Promarak, T. Sudyoadsuk, J. Limtrakul, M. Sawangphruk, Novel hybrid energy conversion and storage cell with photovoltaic and supercapacitor effects in ionic liquid electrolyte, Sci. Rep. 8 (2018) 1–11.
[78] Y.A. Kumar, K.D. Kumar, H.-J. Kim, Reagents assisted ZnCo2O4 nanomaterial for supercapacitor application, Electrochim. Acta 330 (2020), https://doi.org/10.1016/j.electacta.2019.135261.
[79] M.N. Rantho, M.J. Madito, N. Manyala, High-performance symmetric supercapacitor device based on carbonized iron-polyaniline/nickel graphene foam, J. Alloys Compd. (2019) 152993, https://doi.org/10.1016/j.jallcom.2019.152993.
[80] H. Sayahi, M.A. Kiani, S.H. Kazemi, Ultrasonic-assisted synthesis of magnetite/carbon nanocomposite for electrochemical supercapacitor, J. Solid State Electrochem. 18 (2014) 535–543.
[81] T. Zhang, H. Yue, X. Gao, F. Yao, H. Chen, X. Lu, Y. Wang, X. Guo, Polyaniline nanowire arrays on three-dimensional hollow graphene balls for high-performance symmetric supercapacitor, J. Electroanal. Chem. 855 (2019) 113574, https://doi.org/10.1016/j.jelechem.2019.113574.
[82] Y. Zheng, S. Lu, W. Xu, G. He, Y. Cheng, T. Yu, Y. Zhang, The fabrication of graphene/polydopamine/nickel foam composite material with excellent electrochemical performance as supercapacitor electrode, J. Solid State Chem. 258 (2018) 401–409, https://doi.org/10.1016/j.jssc.2017.11.006.
[83] J.S. Shaikh, N.S. Shaikh, R. Kharade, S.A. Beknalkar, J. V Patil, M.P. Suryawanshi, P. Kanjanaboos, C.K. Hong, J.H. Kim, P.S. Patil, Symmetric supercapacitor: sulphurized graphene and ionic liquid, J. Colloid Interface Sci. 527 (2018) 40–48, https://doi.org/10.1016/j.jcis.2018.05.022.
[84] Y. Zhang, G. Wen, S. Fan, Y. Chu, S. Li, B. Xu, J. Zhang, Phenolic hydroxyl functionalized partially reduced graphene oxides for symmetric supercapacitors with significantly enhanced electrochemical performance, J. Power Sources 435 (2019) 226799, https://doi.org/10.1016/j.jpowsour.2019.226799.
[85] P. Tian, J. Zang, S. Jia, Y. Zhang, H. Gao, S. Zhou, W. Wang, H. Xu, Y. Wang, Preparation of S/N co-doped graphene through a self-generated high gas pressure for high rate supercapacitor, Appl. Surf. Sci. 456 (2018) 781–788.
[86] T. Liu, X. Zhang, B. Li, J. Ding, Y. Liu, G. Li, X. Meng, Q. Cai, J. Zhang, Fabrication of Quasi-Cubic Fe_3O_4@ rGO Composite via a Colloid Electrostatic Self-Assembly Process for Supercapacitors, 2014.
[87] L. Wang, C. Wang, H. Wang, X. Jiao, Y. Ouyang, X. Xia, W. Lei, Q. Hao, ZIF-8 nanocrystals derived N-doped carbon decorated graphene sheets for symmetric supercapacitors, Electrochim. Acta 289 (2018) 494–502, https://doi.org/10.1016/j.electacta.2018.09.091.
[88] Y. Chen, Z. Zhang, Z. Huang, H. Zhang, Effects of oxygen-containing functional groups on the supercapacitor performance of incompletely reduced graphene oxides, Int. J. Hydrogen Energy 42 (2017) 7186–7194.
[89] M.M. Mezgebe, Z. Yan, G. Wei, S. Gong, F. Zhang, S. Guang, H. Xu, 3D graphene-Fe3O4-polyaniline, a novel ternary composite for supercapacitor electrodes with improved electrochemical properties, Mater, Today Energy 5 (2017) 164–172.
[90] Y. Zhang, G. Wen, S. Fan, W. Ma, S. Li, T. Wu, Z. Yu, B. Zhao, Alcoholic hydroxyl functionalized partially reduced graphene oxides for symmetric supercapacitors with long-term cycle stability, Electrochim. Acta 313 (2019) 59–69, https://doi.org/10.1016/j.electacta.2019.05.021.
[91] H. Shen, H. Li, M. Li, C. Li, L. Qian, L. Su, B. Yang, High-performance aqueous symmetric supercapacitor based on polyaniline/vertical graphene/Ti multilayer electrodes, Electrochim. Acta 283 (2018) 410–418, https://doi.org/10.1016/j.electacta.2018.06.182.
[92] A. Lewandowski, A. Swiderska-Mocek, L. Waliszewski, Li+ conducting polymer electrolyte based on ionic liquid for lithium and lithium-ion batteries, Electrochim. Acta 92 (2013) 404–411.
[93] D.-L. Lu, R.-R. Zhao, J.-L. Wu, J.-M. Ma, M.-L. Huang, Y.-B. Yao, T. Tao, B. Liang, J.-W. Zhai, S.-G. Lu, Investigations on the properties of Li3xLa2/3-xTiO3 based all-solid-state supercapacitor: relationships between the capacitance, ionic conductivity, and temperature, J. Eur. Ceram. Soc. 40 (6) (2020) 2396–2403.
[94] Y. Han, N. Shen, S. Zhang, D. Li, X. Li, Fish gill-derived activated carbon for supercapacitor application, J. Alloys Compd. 694 (2017) 636–642.
[95] F. Wang, S. Sun, Y. Xu, T. Wang, R. Yu, H. Li, High performance asymmetric supercapacitor based on Cobalt Nickle Iron-layered double hydroxide/carbon nanofibres and activated carbon, Sci. Rep. 7 (2017) 4707.
[96] Y.S. Lim, C.W. Lai, S.B.A. Hamid, Porous 3D carbon decorated Fe 3 O 4 nanocomposite electrode for highly symmetrical supercapacitor performance, RSC Adv. 7 (2017) 23030–23040.
[97] H.R. Naderi, P. Norouzi, M.R. Ganjali, Electrochemical study of a novel high performance supercapacitor based on MnO2/nitrogen-doped graphene nanocomposite, Appl. Surf. Sci. 366 (2016) 552–560.
[98] E. Le Calvez, S. Sathyamoorthi, N. Phattharasupakun, S. Sarawutanukal, M. Sawangphruk, High cell-potential and high-rate neutral aqueous supercapacitors using activated biocarbon: in situ electrochemical gas chromatography, Electrochim. Acta 313 (2019) 31–40.
[99] A.R. Selvaraj, H.-J. Kim, K. Senthil, K. Prabakar, Cation intercalated one-dimensional manganese hydroxide nanorods and hierarchical mesoporous activated carbon nanosheets with ultrahigh capacitance retention asymmetric supercapacitors, J. Colloid Interface Sci. 566 (2020) 485–494, https://doi.org/10.1016/j.jcis.2020.01.117.
[100] V.T. Chebrolu, B. Balakrishnan, V. Raman, I. Cho, J.-S. Bak, K. Prabakar, H.-J. Kim, Co-electrodeposition of NiCu (OH) 2@ Ni-Cu-Se hierarchical nanoparticle structure for supercapacitor application with enhanced performance, Appl. Surf. Sci. 506 (2020) 145015.
[101] C. Venkata Thulasi-Varma, B. Balakrishnan, H.-J. Kim, Exploration of Ni-X (O, S, Se) for high performance supercapacitor with long-term stability via solution phase synthesis, J. Ind. Eng. Chem. 81 (2020) 294–302, https://doi.org/10.1016/j.jiec.2019.09.017.
[102] N. Kularatna, Energy Storage Devices for Electronic Systems: Rechargeable Batteries and Supercapacitors, Academic Press, 2014.
[103] I.M. Mosa, A. Pattammattel, K. Kadimisetty, P. Pande, M.F. El-Kady, G.W. Bishop, M. Novak, R.B. Kaner, A.K. Basu, C. V Kumar, J.F. Rusling, Ultrathin graphene–protein supercapacitors for miniaturized bioelectronics, Adv. Energy Mater. 7 (2017), https://doi.org/10.1002/aenm.201700358.
[104] K. Kongsawatvoragul, S. Kalasina, P. Kidkhunthod, M. Sawangphruk, Charge storage mechanisms of cobalt hydroxide thin film in ionic liquid and KOH electrolytes for asymmetric supercapacitors with graphene aerogel, Electrochim. Acta 324 (2019) 134854.
[105] S.A. Pande, B. Pandit, B.R. Sankapal, Vanadium oxide anchored MWCNTs nanostructure for superior symmetric electrochemical supercapacitors, Mater. Des. 182 (2019) 107972, https://doi.org/10.1016/j.matdes.2019.107972.
[106] H.-C. Jung, R. Vinodh, C.V.V.M. Gopi, M. Yi, H.-J. Kim, Novel composite electrode material derived from hypercross-linked polymer of pyrene and polyaniline for symmetric supercapacitor, Mater. Lett. 257 (2019) 126732, https://doi.org/10.1016/j.matlet.2019.126732.
[107] M.S. Javed, S.S.A. Shah, S. Hussain, S. Tan, W. Mai, Mesoporous manganese-selenide microflowers with enhanced electrochemical performance as a flexible symmetric 1.8 V supercapacitor, Chem. Eng. J. 382 (2020) 122814, https://doi.org/10.1016/j.cej.2019.122814.
[108] D. Moitra, C. Anand, B.K. Ghosh, M. Chandel, N.N. Ghosh, One-dimensional BiFeO3 nanowire-reduced graphene oxide nanocomposite as excellent supercapacitor electrode material, ACS Appl. Energy Mater. 1 (2018) 464–474.
[109] K. Karthikeyan, D. Kalpana, S. Amaresh, Y.S. Lee, Microwave synthesis of graphene/magnetite composite electrode material for symmetric supercapacitor with superior rate performance, RSC Adv. 2 (2012) 12322–12328.
[110] S. Dhibar, A. Roy, S. Malik, Nanocomposites of polypyrrole/graphene nanoplatelets/single walled carbon nanotubes for flexible solid-state symmetric supercapacitor, Eur. Polym. J. 120 (2019) 109203, https://doi.org/10.1016/j.eurpolymj.2019.08.030.
[111] J. Li, X. Li, D. Xiong, L. Wang, D. Li, Enhanced capacitance of boron-doped graphene aerogels for aqueous symmetric supercapacitors, Appl. Surf. Sci. 475 (2019) 285–293, https://doi.org/10.1016/j.apsusc.2018.12.152.
[112] S.S. Balaji, J. Anandha Raj, M. Karnan, M. Sathish, Supercritical fluid assisted synthesis of S-doped graphene and its symmetric supercapacitor performance evaluation using different electrolytes, Synth. Met. 255 (2019) 116111, https://doi.org/10.1016/j.synthmet.2019.116111.
[113] J. Zhu, S. Dong, Y. Xu, H. Guo, X. Lu, X. Zhang, Oxygen-enriched crumpled graphene-based symmetric supercapacitor with high gravimetric and volumetric performances, J. Electroanal. Chem. 833 (2019) 119–125, https://doi.org/10.1016/j.jelechem.2018.11.032.